2016

The Role of RNASE L in Type I Diabetes and Development of Quantitative LC-MS/MS Methods for the Pharmacological Studies of Anti-Cancer Drug Candidates

Chun Zeng

THE ROLE OF RNASE L IN TYPE I DIABETES AND DEVELOPMENT OF QUANTITATIVE LC-MS/MS METHODS FOR THE PHARMACOLOGICAL STUDIES OF ANTI-CANCER DRUG CANDIDATES

CHUN ZENG

BACHELOR OF SCIENCE IN BIOLOGY

UNIVERSITY OF SCIENCE AND TECHNOLOGY OF CHINA

JULY 2005

Submitted in partial fulfillment of requirements for the degree

DOCTOR OF PHIOLOSOPHY IN CLINICAL-BIOANALYTICAL CHEMISTRY

at the

CLEVELAND STATE UNIVERSITY

APRIL 2013

We hereby approve this thesis/dissertation for

Chun Zeng

Candidate for the

DOCTOR OF PHILOSOPHY IN CLINICAL AND BIOANALYTICAL CHEMISTRY

for the Department of Chemistry and

CLEVELAND STATE UNIVERSITY'S

College of Graduate Studies by

Dissertation Chairperson, Dr. Aimin Zhou

Department/ Date

Dr. David Anderson

Department/ Date

Dr. Baochuan Guo

Department/ Date

Dr. Xue-Long Sun

Department/ Date

Dr. Anton A. Komar

Department/ Date

Date of Defense
April 30th, 2013

ACKNOWLEDGEMENTS

I would like to express my appreciation to my mentors, friends and family members for the continuous guidance and support along with my Ph.D. study.

First, I wish to thank Dr. Aimin Zhou, my advisor, for his guidance, support, encouragement, understanding and kindness that helped me complete this research. I have always admired Dr. Zhou's extraordinary diligence, accountability, enthusiasm, friendliness and patience and he has inspired me in so many ways.

I would like to express my special appreciation to Dr. David J. Anderson, for his help, support, advice, encouragement, understanding, kindness and patience. I admire Dr. Anderson's helpfulness, outgoingness and care. He has been a devoted teacher, and a very pleasant person.

I would like to express my gratitude to my committee members, Dr. Baochuan Guo, Dr. Xue-long Sun, and Dr. Anton A. Komar, who have given precious suggestions on my research.

I would like to thank Dr. Xiang Zhou for training me on instrumentation, offering me a great opportunity to work as an instrumentation assistant.

I would like to express many thanks to my colleagues in Dr. Zhou's lab: Drs. Haiyan Tan, Xin Yi, Lin Zhang and Mr. Boo Seok Yun. I enjoy the friendly working environment and appreciate their technical help, group discussion and friendship.

I would like to thank Ms. Richelle Emery and Mrs. Michelle Jones for their help with the administrative affairs at CSU.

Finally, I would like to express my thanks to my family and friends.

THE ROLE OF RNASE L IN TYPE I DIABETES AND DEVELOPMENT OF QUANTITATIVE LC-MS/MS METHODS FOR THE PHARMACOLOGICAL STUDIES OF ANTI-CANCER DRUG CANDIDATES

CHUN ZENG

ABSTRACT

PROJECT I:

The cause of type I diabetes continues to be a focus of investigation. In this study, we found that 2-5A dependent RNase L (RNase L), an IFN-α-inducible enzyme that functions in IFN action against viruses and cell proliferation, played an important role in dsRNA-induced onset of type I diabetes. By using RNase L deficient RIP-B7.1 mice which are more vulnerable to environmental harmful factors such as viral infection, we demonstrated that deficiency of RNase L in mice resulted in a significant delay of diabetes onset induced by polyinosinic:polycytidylic acid (poly I:C), a type of dsRNA, and streptozotocin (STZ). Immunohistostaining showed that the population of infiltrated CD8+ T-cells was remarkably reduced in the islets of RNase L deficient mice, implicating RNase L may contribute to type I diabetes onset through regulating immune responses. Furthermore, RNase L was responsible for the

expression of certain proinflammatory genes in the pancreas under the special condition.

PROJECT II:

It has been found that 6-hydroximino-4-aza-A-homo-cholest-3-one (HyM3) is a steroidal derivative with a significant anticancer effect.

To develop a method for analyzing its pharmacological kinetics, HyM3 and the internal standard (3E)-Hydroximinocholest-6-one were extracted from mouse plasma samples through a protein precipitation procedure by mixing with acetonitrile (1:4 v/v) and then centrifuging at 12,400 g for 15 minutes. The supernatant (10 μl) was injected onto the LC/MS system consisting of a Shimadzu Prominence HPLC and an AB Sciex QTrap 5500 with positive electrospray ionization. A MRM mode was chosen for sensitive and specific detection of the analyte and internal standard. The HPLC separation employed a Phenomenex Kinetex C8 column (50x2.1 mm, 2.6μ) with a gradient mobile phase of 0.2% formic acid in water and 0.2% formic acid in acetonitrile at a rate of 0.2 ml/min. Full mass spectrometric scans of HyM3 and the internal standard showed protonated molecular ions of 431 and 416 m/z, and fragmentation of these two ions revealed predominant product ions of 370 m/z and 344 m/z respectively. HyM3 was retained on the HPLC column for 6.4 minutes, while the internal standard was retained for 7.3 minutes. The method was calibrated for a concentration range from 0.500 to 200 ng of Hym3 per mL of plasma.

TABLE OF CONTENTS

LIST OF TABLES

LIST OF FIGURES

LIST OF ABBREVIATIONS

2–5A 2’-5’ oligoadenylates

ANK ankyrin repeats

AR androgen receptor

cDNA: complementary deoxyribonucleic acid

CE Collision Energy

CSF-1R colony-stimulating factor 1 receptor

CXP Cell Exit Potential

dsRNA double-stranded RNA

DP Declustering Potential

EGF epidermal growth factor

EMCV encephalomyocarditis virus

ERK extracellular signal-regulated kinase

EI Electron impact ionization

EP Entrance Potential

ESI Electrospray ionization

FBS fetal bovine serum

FDA U.S. Food and Drug Administration

FRET fluorescence resonance energy transfer

GAS gamma IFN-activated site

Grb 2 growth factor receptor-bound protein 2

HIV-1 human immunodeficiency virus type 1

HPC hereditary prostate cancer

HSV-1 herpes simplex virus type 1

IFN interferon

IL-1β interleukin 1 β

IL-6 interleukin 6

ISGs IFN-stimulated genes

ISRE IFN-stimulated regulatory element

ITIM immuno receptor-tyrosine based inhibitory motif

JAKs Janus kinases

JNK c-Jun NH2-terminal kinase

Kb kilo-base pair

LBP LPS-binding protein

LPS lipopolysaccharide

LC-MS/MS Liquid chromatography-tandem mass spectrometry

MAPK mitogen-activated protein kinase

LOD Limit of detection

LLOQ Lowest limit of quantification

LOQ Limit of quantification

MALDI Matrix-assisted laser desorption/ionization

MeCN Acetonitrile

MeOH Methanol

MS Mass spectrometry

MEFs mouse embryonic fibroblasts

mRNA messenger ribonucleic acid

NGF nerve growth factor

NSAIDs nonsteroidal anti-inflammatory drugs

PAGE polyacrylamide gel electrophoresis

PBS phosphate buffer saline

PCa prostate cancer

PCR polymerase chain reaction

PDGF platelet-derived growth factor

PGs prostaglandins

PIV-3 human parainfluenza virus-3

MRM Multiple reaction monitoring

M/Z Mass/charge ratio

NAD+ Oxidized nicotine amide adenine dinucleotide

PKC protein kinase C

PKR double-stranded RNA dependent protein kinase R

PLC phospholipase C

PMA phorbol ester

RNA ribonucleic acid

RNase L ribonuclease L

rRNA ribosomal RNA

S/N ratio Signal-to-noise ratio

TOF Time of flight

UV/VIS Ultra-violet / visible light

RT-PCR reverse transcription PCR

SAPK stress-activated protein kinase

SDS sodium dodecyl sulphate

SiRNA small interfering RNA

TNF-α tumor necrosis factor alpha

CHAPTER I

INTRODUCTION

Project I: The role of RNASE L in type I diabetes and renal function

1.1 Overview of Type I Diabetes mellitus (DM)

Diabetes mellitus is associated with a variety of complications including blindness, kidney failure, heart disease, painful nerve damage, and circulatory problems so severe they necessitate amputation [1-4]. The Centers for Disease Control and Prevention (CDC) reported in 2011 that more than 25.8 million Americans—8.3% of the population—have diabetes. This number is predicted to be doubled in the next two decades [5]. There are two types of diabetes: insulin-dependent diabetes mellitus (IDDM) or juvenile-onset diabetes and non-insulin-dependent diabetes mellitus (NIDDM). Diabetes costs the nation about $245 billion in 2012 [6].

1.1.1 Epidemiology of DM

Diabetes mellitus is caused by inherited and/or acquired deficiency in insulin production by the pancreas, or by the ineffectiveness of the insulin produced. Such deficiency or ineffectiveness results in increased concentrations of blood glucose, which in turn damages many of the body's system, in particular the blood vessels and nerves. Type 1 and type 2 diabetes are the main forms of diabetes.

As one of the most common non-communicable disease worldwide, diabetes is one of the most challenging health problems in the 21st century. In most developed countries, diabetes is the fourth or fifth leading cause of death. Substantial evidence shows that it is also epidemic in many developing countries. The incidence of diabetes is increasing greatly worldwide. And this trend is likely to keep going in the future decades. (Figure 1-1 and figure 1-2)

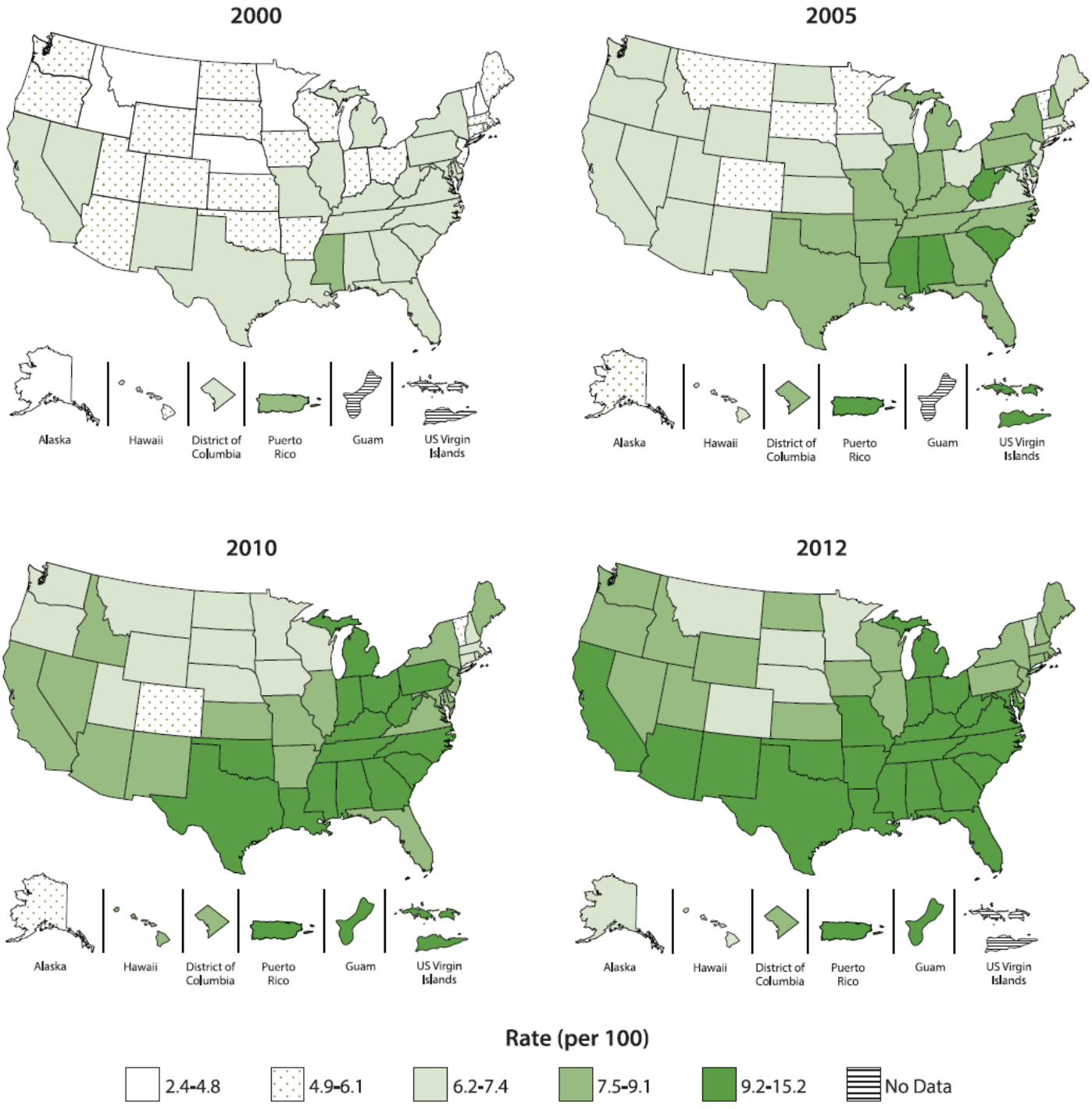

Figure 1-1.The tread of the diabetes from 2000 to 2012, data from the Diabetes report card, 2014

Diagnosed and undiagnosed diabetes among people aged 20 years or older, United States, 2012

	Number with diabetes (millions)	Percentage with diabetes (unadjusted)
Total		
20 years or older	28.9	12.3
By age		
20–44	4.3	4.1
45–64	13.4	16.2
65 years or older	11.2	25.9
By sex		
Men	15.5	13.6
Women	13.4	11.2

Source: 2009–2012 National Health and Nutrition Examination Survey estimates applied to 2012 U.S. Census data.

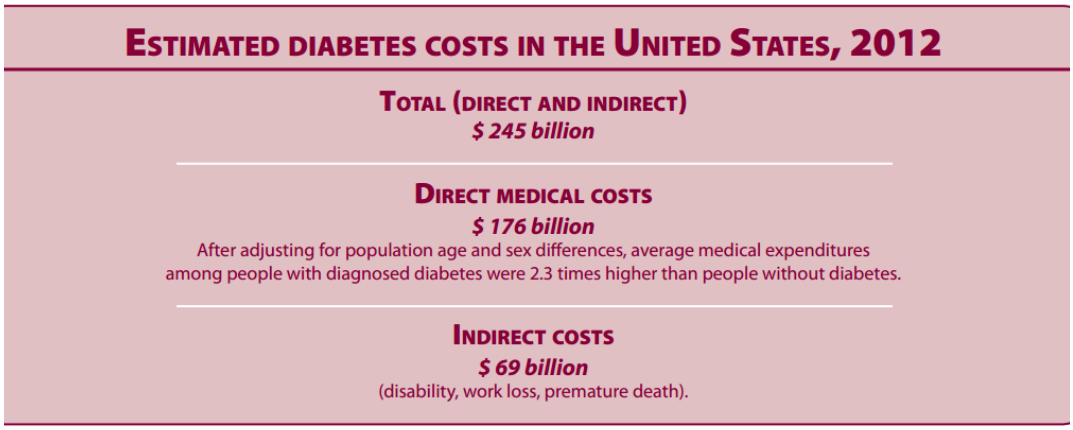

Figure 1-2. Data from the National Diabetes Statistics Report, 2014

1.1.2 The etiology of TIDM

The etiology of diabetes (Figure 1-3) continues to be a focus of investigation. Both genetic and environmental factors such as toxins, viruses, and diets are believed to

play an important role in its pathogenesis [7]. A reduction of insulin producing pancreatic β-cells has been considered as one of the key factors in the development of diabetes, particularly in type I diabetes [8,9]. In type I diabetes, autoimmunological destruction of the pancreatic β-cells results in an absolute loss of insulin production. Investigation of the molecular mechanisms underlying β-cell destruction has revealed that microbial infections recruit immune effectors mediating β-cell apoptosis, which in turn triggers autoimmune responses [9]. The NOD mouse is an ideal model of spontaneous type I diabetes, a T cell-mediated autoimmune disease. Histological studies have shown that infiltration of immune cells including macrophages and lymphocytes around the islets starts at 3 to 4 weeks of age, causing insulitis [10,11]. The role of $CD4^+$ and $CD8^+$ T-cells in the onset of type I diabetes has been well established in recent years. Clinical and animal studies have shown that $CD8^+$ T cells take a central stage in the destruction of pancreatic β-cells and contribute to sustaining islet inflammation, leading to the onset of type I diabetes [10-13].

The expression of proinflammatory genes has been implicated in the pathogenesis of type I diabetes [14]. In NOD mice, an increased expression of IFN-γ, TNF-α and IL-1β is associated with β-cell destructive insulitis [10, 11]. In recent years the role of IFN-α in autoimmune diseases including type I diabetes has been well established [15]. Increased levels of IFN-α in the sera of type 1 diabetes patients have been documented [16]. Transgenic mice expressing IFN-α in the β-cells develop

hypoinsulinemic diabetes associated with a mixed inflammation centered on the islet, which can be prevented with a neutralizing antibody to IFN-α [17]. It has been reported that the onset of type I diabetes in both the BB rat and STZ-treated mice is IFN-α dependent [18]. In addition, IFN-α also mediates induction of type I diabetes by poly I:C in the mice expressing the B7.1 costimulatory molecule on β-cells in islets [19]. Most recently, a study has revealed that blockade of IFN-α signaling by anti-IFNAR1 in 2- to 3-week old NOD mice remarkably delays the onset and decreases the incidence of diabetes, suggesting the involvement of IFN-stimulated genes in the pathogenesis of type I diabetes [20] (Figure 1-4 and 1-5).

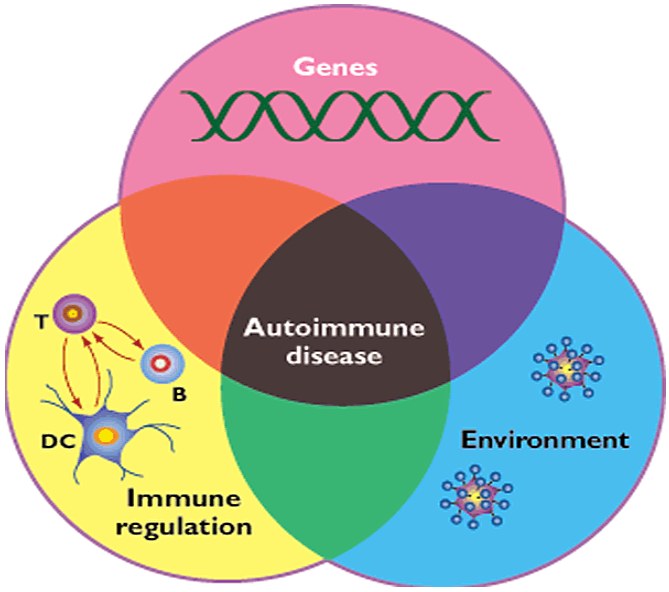

Figure 1-3. The etiology of diabetes. (**E**rmann *et al* , Nat Immunol. 2001)

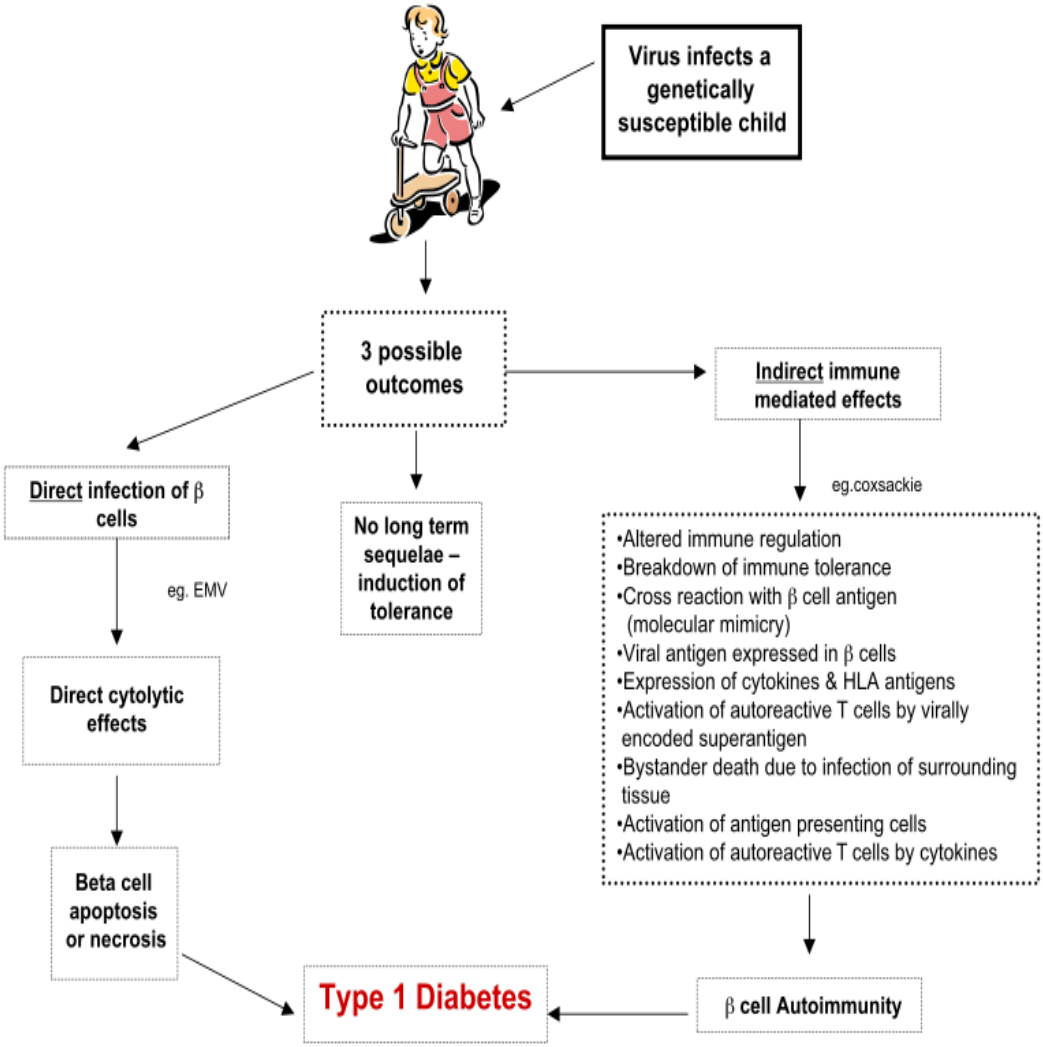

Figure 1-4. Mechanisms of viral-induced type I Diabetes. (D. Devendra and G.S. Eisenbarth Clinical Immunology. 2004)

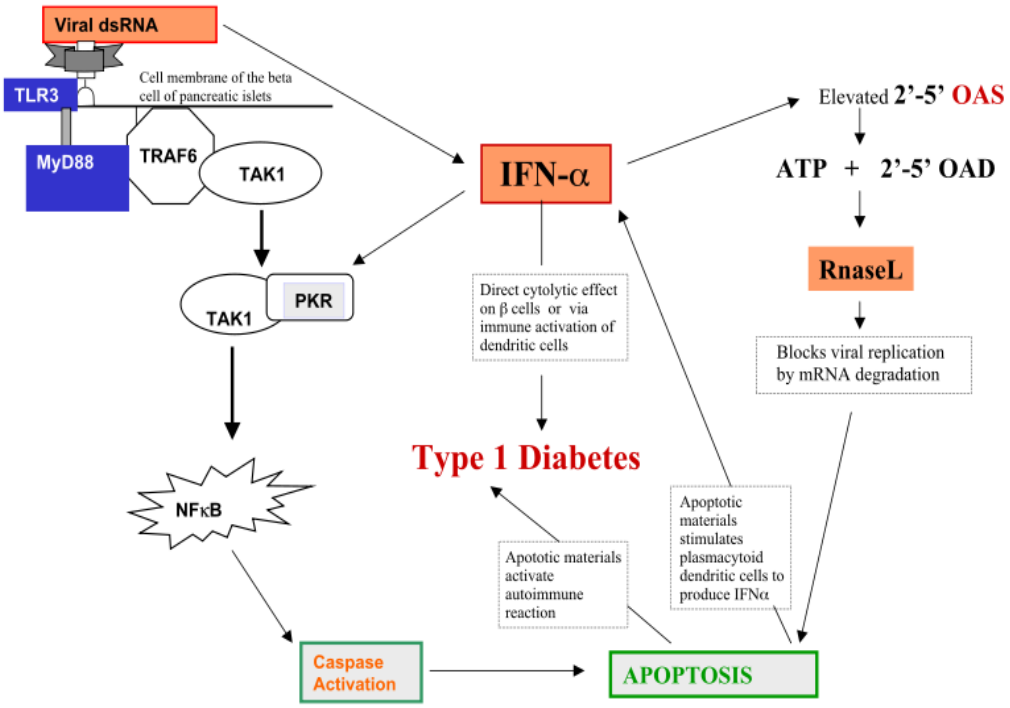

Figure 1-5. The effect of viral dsRNA and interferon alpha on the pathogenesis of type I diabetes. (D. Devendra and G.S. Eisenbarth Clinical Immunology. 2004)

1.2 Introduction of IFN

1.2.1 Type I IFN

Human type I IFNs comprise a vast and growing group of IFN proteins such as IFN-α, IFN-β, IFN-κ, IFN-δ, IFN-ε, IFN-τ, IFN-ω and IFN-ζ. Type I IFNs are encoded by a gene cluster located on the short arm of chromosome 9 in humans and chromosome 4 in mice. A map of the type I IFN gene contains 26 IFN genes and pseudogenes [21]. IFN-α that is produced by peripheral leukocytes (B cells and T-cells) and IFN-β that is secreted by fibroblasts, are both the most studied subfamilies of type I IFN and both

of them can be induced in mammalian cells in response to viral infection. All IFN-α genes encode for the same size primary proteins with 166 amino acids in length, except IFN-α2 that encodes for 165 amino acids [22]. No evidence was found for the existence of an intron, in either the coding or the non-coding segments of the gene [21]. IFN-α subfamily is up to 70% homologous at the protein level and from 80%-100% at the nucleotide level. IFN-β shows from 25%-30% homology with the IFN-α subfamily members at amino acid levels and 45% at the nucleotide level [23]. Type I IFNs bind to a specific cell surface receptor complex that consists of IFNAR1 and IFNAR2.

1.2.2 Type II IFN

INF-γ is the only member in type II IFN. The mature IFN-γ ligand is an anti-parallel homodimer, and it binds to the IFN-γ receptor complex, which is made up of two of each IFNγR1 and IFNγR2 subunits. It is produced in activated T-cells and natural killer cells [24]. Human IFN-γ is a 146 amino acids protein N-glycosylated at two sites and encoded on four exons, in contrary to intronless type I IFN[25]. The IFN-γ gene is located on chromosome 12 in humans and chromosome 10 in mice. IFN-γ is involved in the regulation of the immune and inflammatory responses. It is released by Th 1 cells and recruits leukocytes to a site of infection, resulting in increased inflammation. It also stimulates macrophages to kill bacteria that have been engulfed. IFN-γ has

some anti-viral and anti-tumor effects, but these are generally weak; it, however, potentiates the effects of IFN-α and IFN-β.

1.2.3 The signal transduction of IFNs

IFNs bind to completely different cell surface receptors; however, the signal transduction pathways activated by the IFN-α/β and IFN-γ receptors partially overlap. IFNs exert their actions through cognate cell surface receptors that are largely species specific [26]. The α, β, and ω IFNs appear to have a common receptor consisting of two subunits, IFNAR-1 and IFNAR-2. Binding of IFN α/β initiates the signaling cascade by causing dimerization of the receptor subunits, IFNAR1 and IFNAR2. This initial step triggers a conformation change that is propagated through the cell membrane and is responsible for the initiation of the phosphorylation cascade. IFN-mediated the signaling and transcriptional activation of cellular gene expression are best understood in the context of JAK-STAT pathway [27]. There are seven known members of the signal transducer and activator of transcription (STAT) family of proteins, Stat-1, Stat-2, Stat-3, Stat-4, Stat-5a, Stat-5b, and Stat-6, and four members of the Janus family of tyrosine kinase (JAK) enzymes, Jak-1, Jak-2, Jak-3, and Tyk-2. STATs are latent cytoplasmic transcription factors that become tyrosine phosphorylated by the JAK in response to cytokine stimulation. Different members of the JAK and STAT families have distinct functions in cytokine signaling. Of the known JAKs and STATs, the Jak-1, Jak-2, and Tyk-2 kinases and the Stat-1 and

Stat-2 transcription factors play central roles in mediating IFN-dependent biological responses, including induction of the antiviral state [28]. The first intracellular component of the signaling pathway that receives the "transduction pulse" is the JAK kinase, Tyk2, which is pre-associated with IFNAR1. Upon interferon stimulation, Tyk2 is immediately phosphorylated by JAK1, another JAK kinase, which is bound to IFNAR2. Activated Tyk2 then in turn phosphorylates JAK1. The activated JAK kinases, Tyk2 and JAK1, are responsible for the subsequent phosphorylation of IFNAR1 and IFNAR2 at specific tyrosine residues. STAT2 then binds to specific phosphorylated residues on IFNAR1. Upon docking, STAT2 is phosphorylated at a conserved tyrosine residue (Y701) by the JAK kinases thereby creating an additional docking port for STAT1, which is also subsequently phosphorylated at Y690. The phosphorylated STATs then dissociate from the receptor heterodimer and bind to p48 (IRF9), a member of the IFN regulatory factor (IRF) family, forming the major IFN transcription factor, known as ISGF-3. ISGF-3 translocates to the nucleus and binds to specific regulatory DNA sequences (ISRE-IFN stimulated response elements) and initiates transcription of IFN-inducible genes.

1.3 IFN-induced genes associated with its antiviral function

IFNs display their biological function via inducing IFN-stimulated genes (ISGs). The well-studied ISGs associated with its antiviral action of IFNs are dsRNA-dependent

protein kinase R (PKR), the 2'-5'oligoadenylate synthetase (OAS), RNase L, the Mx protein GTPases [27].

1.3.1 Mx proteins

Mx proteins are synthesized in IFN-treated vertebrate cells. The name of these proteins comes from their ability to inhibit the replication of myxoviruses, such as influenza. In human, Mx gene products are designated as MxA, and MxB, whereas in rat and murine species Mx gene products are designated as Mx1, Mx2, and Mx3. The location of Mx proteins in specific compartments is related to their biological function. Mx1 proteins are nuclear proteins and as a consequence of their location, they inhibit influenza virus in the nucleus. The mechanism of how Mx proteins inhibit the replication of different viruses is unknown. Proteins MxA and Mx1 of the Mx family of proteins are possibly the best characterized of the known IFN-inducible gene products with antiviral activity. It has been established that Mx alone is sufficient to block the replication of virus in the absence of any other IFN α/β-inducible proteins [27]. Mx proteins are GTPases that belong to the superfamily of dynamin-like GTPases [29]. The intrinsic GTPase activity of Mx proteins is required for their antiviral activity. The highly conserved tripartite GTP binding motif is present within the N-terminal region of the 70- to 80-kDa proteins. Mx proteins associate with themselves and, importantly, with viral protein complexes. The central and C-terminal regions of Mx play important roles in these protein-protein interactions [30]. Mx is inducible by

IFN-α and IFN-β but not by IFN-γ [31]. The Mx proteins [32] plays a pivotal roles in inhibiting two members of the Orthomyxoviridae family: influenza virus and Thogoto virus. The human genome contains two related Mx proteins, MxA and MxB, which are induced by IFN-α/β. The human MxA protein has 662 amino acids whereas the MxB protein has 715 amino acids. Both human MxA and MxB are mapped to chromosome 21. The MxA protein normally accumulates in the cytoplasm of IFN-treated cells and possesses antiviral activity. The antiviral activity of MxA, which undergoes oligomerization, is dependent upon GTP binding and hydrolysis. Cells that constitutively express the human MxA protein show a high degree of antiviral activity, displaying resistance to several members of the Orthomyxoviridae including influenza A and C viruses and Thogoto virus. Interestingly, a number of additional RNA viruses including members of the Bunyaviridae (LaCrosse virus, Hantavirus), Paramyxoviridae (measles virus, parainfluenza 3), Rhabdoviridae (VSV), and Togaviridae (Semliki Forest virus) are inhibited by MxA expression either in cultured cells or in transgenic mice [27].

1.3.2 PKR

The pkr gene encoding the IFN-inducible, RNA-dependent protein kinase, PKR, was isolated as lambda phage and P1 phage clones from human genomic DNA. The genomic nucleotide sequence revealed 17 exons encoding the 551–amino acid PKR protein [33]. PKR was known in the earlier literature as DAI or dsI; P1 kinase;

P1/eIF-2α kinase; p65, p67, or TIK (for the mouse enzyme); and p68 or p69 (for the human enzyme) [27]. In IFN-treated cells, PKR is found predominantly in the cytoplasm and associated with ribosomes; however, small amounts of PKR have also been localized to the nucleus. The expression of PKR is rapidly stimulated by IFNs and reaches levels approximately 5-10 folds higher than that in resting cells. This action of IFN is mediated through an ISRE (IFN-stimulated regulatory element) and GAS (gamma IFN-activated site) in the promoter region of the PKR gene. PKR contains two conserved dsRNA-binding motifs at the amino-terminus, RI (amino acids 55-75) and RII (amino acids 145-166). Both regions possess a similar core sequence, but RI alone appears to be necessary and sufficient to mediate dsRNA binding. It is believed that a combination of both domains creates a single binding site where the different domains bind to different regions of the dsRNA molecule [27]. No RNA sequence specificity has been identified. PKR is activated by double stranded RNA (viral RNA or secondary RNA structures), which results in a conformational change that uncovers the carboxyl-terminal catalytic domain of PKR. Approximately 50 bp of duplexed RNA are required for its full activation, although shorter stretches of secondary structure on pre-dominantly single stranded RNA can activate PKR. This activates the kinase activity of PKR, which then undergoes autophosphorylation/activation in several serine and threonine residues. The activated kinase phosphorylates in turn the translation initiation factor eIF2-α at Ser51, resulting in inhibition of viral protein synthesis [34].

1.3.3 The 2-5A system

The 2-5A system is an RNA degradation pathway that can be induced by IFNs. The system consists of two IFN-inducible enzymes: 2-5A synthetase (OAS) and RNase L [35]. IFNs interact with cell surface receptors to activate a set of genes through the JAK-STATs signal transduction pathway, some of which encode several 2-5 A synthetases that are dsRNA dependent. In general, dsRNA is produced during viral infection. DsRNA activates 2-5 A synthetases that can use intracellular ATP to synthesize 2-5A that is a unique group of heat-stable, 5'-phosphorylated, 2'-5'-phosphodiester-linked oligoadenylates, with general formula ppp(A2'p5')nA (n≥2). The 2'- 5' phosphodiester linkage is unusual in contrast to the typical 3'- 5' linkage present in RNA and DNA chains. 2-5A binds RNase L with high affinity, converting it from its inactive, monomeric state to a potent dimeric endoribonuclease, thus leading to the interruption of many fundamental processes which are essential for cell function and virus replication (Figure 1-6). Cells over expressing RNase L overcome viral infection, while over expression of a dominant mutant of RNase L results in an increase of the susceptibility to viral infection. The role of 2-5 A system as a host defense against some types of viruses is well established, but additional possible biological roles of the 2-5A system, such as in cell growth and differentiation, heat shock, atherosclerotic plaque, pathogenesis of type I diabetes, and apoptosis were also reported [36].

1.4A 2-5A Synthetase (OAS)

OAS activity has been demonstrated to be present in cells from mouse to humans, even in reptiles and several avian species. OAs catalyzes the following reaction:

$$(n+1)\ ATP \xrightarrow[dsRNA]{Mg\ 2+} pppA\ (2\ 'p5'A)\ n + n\ PPi \qquad (n = 2\ to\ 15)$$

A number of growth factors can induce the expression of OAS. Epidermal growth factor can induce a 3-to 5-fold increase of OAS in human fibroblastomas, while PDGF induces OAS in murine BALB/c3T3 cells. NGF increases the expression of OAS from 5- to 25- folds in the rat pheochromocytoma cell line (PC12) [37]. Cyclic AMP also enhances the OAS mRNA at the transcriptional level [38]. IFN-α, IFN-β and IFN-γ all are able to induce an increase in OAS activity. Interestingly it has been found that a given IFN subtype can differentially induce specific isoforms of OAS. In Hs294t melanoma cells, after treatment with IFN-α, the isoform p40 was induced to twice the extent of p100 [39]. In contrast, IFN-γ induced both isoforms equally. The induction of p69 and p100 isoforms by IFN-γ has been studied in Daudi, fibroblast, and colon adenocarcinoma cells *in vitro* and *in vivo* and there were significant differences in induction between cell types [40]. The OAS activity has been found in a variety of cell types during differentiation. Differentiation of skeletal muscle cells in several species has been found to be associated with OAS induction and 2-5A formation. Cell differentiation induced by chemicals or cytokines has been associated with an increase of the OAS level. A 27-fold increase in the expression of OAS was

observed in human HL-60 cells after treatment with dimethyl sulfoxide [41]. Induction of differentiation in U937 cells by hydroxyvitamin D3 was associated with IFN production and an increase in OAS [42]. On the other hand, OAS activity has been found to be low in normal proliferating diploid Syrian hamster (FC13) cells [43]. Taken together, all suggest a role of OAS in the anti-proliferative effects of IFN. Levels of OAS depend also on a phase of the cell cycle. Using mouse embryo tertiary fibroblasts progressing synchronously through the cell cycle as determined by fluorescence-activating cell sorting, OAS levels were found to be low in quiescent cultures, as well as during G1 and early S. They then rose 10-fold in late S and decreased sharply in G2 [44]. A similar, though quantitatively a lower pattern, was found for RNase L. High OAS levels result in the inhibition of EMCV, mengovirus, and vaccinia replication. Mammalian OAS is an important mediator of the antiviral activity of IFNs. The existence of distinct 69- and 100-kDa forms of OAS, in addition to the smaller (40 and 46 kDa) forms, has been established. Both human and mouse 2-5A synthetase gene families encode four forms of enzymes. The human p40-46 forms are coded for by 1.6 and 1.8 kb mRNAs, which are derived from the same gene through cell type-specific differential splicing between the 7th and an additional 8th exon of this gene, which is localized to chromosome 12 [45] . The p40 and p46 OAS isoforms are localized in nuclei. p69 OAS was localized in cytoplasm but it was found in closer association with the nuclear membrane [46]. P100 is localized in cytoplasm [36]. Interestingly, OAs is persistently activated in patients with type 1 diabetes, suggesting the involvement of the 2-5A system in the disease [47].

1.4B RNase L

RNase L is a unique ribonuclease because it requires an unusual allosteric effector, 2-5A, to catalyze the cleavage of single-stranded RNA [15]. 2-5A was discovered [48] in extracts of IFN treated cells in the presence of dsRNA and ATP [49]. RNase L is found in mammalian cells from mouse to humans, but not in fish, insects, plants and bacteria [50]. In mice, RNase L is highly expressed in the spleen, lung, liver, and kidney at 5 days of age and then decrease with age, except in the spleen where it remains high until adulthood [51]. RNase L is localized in the nuclei and cytoplasm [52]. Its levels were found to be elevated during cell differentiation, as well as in growth arrested cells [53]. Additionally, introduction of 2-5A into cells impaired cell growth [54]. Surprisingly, the increased RNase L levels were found in colorectal cancer tissues although its role in the pathogenesis of this disease is largely unknown [55]. Human and murine RNase L has been successfully cloned [[22]]. Many computer-assisted homology searches, deletion analysis and site directed mutagenesis revealed the structural and functional domains of RNase L (Figure 1-7). RNase L consists of three domains, namely the N-terminal ankyrin domain, the protein kinase homology domain, and the C-terminal ribonuclease domain. The N-terminal ankyrin repeat domain, a region containing nine ankyrin-like macromolecular recognition repeats (the ninth ankyrin repeat is incomplete), is responsible for 2-5A binding, and the C-terminal domain is responsible for catalytic activity [56].

B.1 Structure of 2-5A dependent RNase L

A successful molecular cloning of murine and human RNase L by Zhou and Hassel [57] opened the door to the structural analysis of the enzyme. The sequence of full-length human RNase L was obtained from a composite cDNA (HZB1) genomic construct. Human RNase L gene encodes a sequence of 741 amino acids (m.w. 83,539 kDa) with unique structural and functional motifs (Figure. 1-7). In the presence of 2-5A activators, RNase L dimerizes to form catalytically active enzyme [58]. There are a group of negatively charged amino acids from positions 451-459 and a positively charged group at 677-684, and the composition of human RNase L is greater than one-third charged amino acid residues with 113 aspartic acids plus glutamic acids and arginine plus lysines; however the significance of the charge distribution is unknown. A bipartite model for the structure of RNase L emerged in which the regulatory functions of the molecule are located in the N-terminal half, whereas the catalytic domain is present in the C-terminal half [59]. RNase L contains:

Ankyrin repeats

The analysis of the sequence of RNase L revealed that N-terminal 330 residues contained 9 ankyrin (ANK) repeats, with an average length of 33 residues with 35% sequence homology to human erythrocyte ANK [58]. The ninth ankyrin repeat is incomplete. It has been reported that the crystal structure of the N-terminal ankyrin repeat domain (ANK) of human RNase L is associated with the 2-5A binding [56]. This finding was the first structural view of an ankyrin repeat structure directly

interacting with a nucleic acid, rather than with a protein. According to the paper, the ANK domain folds into eight ankyrin repeat elements and forms an extended curved structure with a groove running across the long concave surface. Each repeat is formed by ~33 amino-acid residues and consists of pairs of antiparallel α-helices stacked side by side, which are connected by a series of intervening β-hairpin motifs. The 2-5A molecule is accommodated at a concave site and directly interacts with ankyrin repeats 2–4. The structural basis for 2-5A recognition by ANK is essential for designing stable 2-5A with a high likelihood of activating RNase L. It is believed that 2-5A binding could induce a conformation change in the enzyme that releases an internal clamp on the catalytic domain imposed by ankyrin repeats. Presumably, 2-5A binding could result in the unmasking of an interaction domain, permitting dimerization and activation of RNase L [35]. Fluorescence spectra of RNase L showed clear difference in the presence and absence of 2-5A [60]. The alterations in spectra supported conformation changes of the protein. Time-resolved anisotropy measurements indicated that 2-5A binding led to a significant decrease in the rotational radius of the protein. In addition, 2-5A provides the domain with resistance to protease digestion as a result to conformational change. These results indicate that the ankyrin-repeat domain of RNase L constricts its structure by binding of 2-5A [60]. Ankyrin repeats are highly conserved protein/protein interaction domains, that are present in the amino-terminal half of the enzyme. Proteins that contain ankyrin repeats function in transcriptional control, cell cycle regulation, and differentiation [61], but the function of these repeats in RNase L has never been addressed, although a

controlling role of them in dimerization and activation of the enzyme has been suggested [57]. RNase L is the only nuclease known to contain ankyrin repeats.

Duplicated P-loop-like motif

Duplicated P-loop-like motif (GLY-LYS-THR) was implicated in mediating 2- 5A binding [57]. Two P-loop motifs have been localized between amino acids 218 and 294. Substitution of both lysines in p-loop, at position 240 and 274, with aspargines diminished the binding ability for 2-5A [59]. The result suggested that lysines played a crucial role in the sequence and they were considered the key amino acids that interacted with phosphate groups of nucleotides. Ankyrin repeats 7th and 8th were implicated in 2-5A binding until it was established [56] that 2nd and 4th ankyrin repeats were responsible for the binding according to its crystal structure. RNase L interacts *in vivo* with RLI protein, its inhibitor that does not show any significant homologies with RNase L except that both proteins contain two P-loop motifs. The RLI gene was localized to locus 4q31 by in situ hybridization indicating that this gene and other enzymes of the 2-5A pathway are not organized in cluster in the human genome [62]. RLI cDNA codes a 68-kDa polypeptide which expression is not regulated by IFN [63].

B.1.3 Cysteine rich region within a protein kinase homology is in the C-terminal half of the enzyme but its kinase activity has never been detected. On the basis of a computer-assisted analysis, it was proposed that RNase L was a functional active protein kinase because it matches 11 typical protein kinase domains [64]. However, some of the proposed protein kinase domains in RNase L are either incomplete or differ significantly from known protein kinase domains. It is believed that RNase L has significant homology in its C-terminal half with protein kinase domains VI and VII and some additional homology to other protein kinase domains, especially with domain II [35]. It would appear that RNase L is evolved, at least in part, from a protein kinase. The similarity is due to evolutionary convergence to gain functions in common with protein kinases, such as ATP binding activity [57]. In protein kinases, the conserved lysine in domain II functions in binding to the α- and β- phosphoryl groups of ATP and the conserved aspartate in domain VII chelates Mg^{2+} complexed with ATP [35]. Both of these amino acids present in the protein kinase homology region of RNase L as well. Within the protein kinase homology region of RNase L a high-cysteine-content region is present [57]. Residues 401-436 in human RNase L, and residues 395-444 in murine RNase L, bear resemblances to some zinc fingers, protein/nucleic acid-binding domains [65], suggesting a role in RNA binding. Because zinc is known to inhibit the catalytic activity of RNase L, it is difficult to explain the function of the cysteine-rich region [58]. On the basis of deletion-mutant analysis [59], the region between Glu711 and His 720 was revealed to be essential for RNA binding.

Scanning mutagenesis examination indicated that both Tyr 712 and Phe 716 provide the enzyme with a RNA binding activity [66].

B.2 Localization of the RNase L gene

The gene for RNase L, designated RNS4, maps to human chromosome 1q25 by fluorescence in situ hybridization [67], that is deleted or rearranged in prostate and breast cancer cells, and some gastric adenocarcinomas and oral squamous cell carcinomas [68, 69].

B.3 RNase L antiviral activity

The classical IFN-dependent antiviral response to viral infection involves the regulation of IFN-stimulated genes (ISGs), one being the gene encoding cellular endoribonuclease RNase L, which inhibits protein synthesis and induces apoptosis by cleaving rRNA [70]. Considerable evidence exists relating RNase L to the antiviral activity of IFN [16]. EMCV, a cardiovirus, that is a member of Picornaviruses and causes mild febrile illness in a number of species, including humans, has been often evaluated in conjunction with the 2-5A system. Accumulation of 2-5A as measured by rRNA cleavage has been observed in EMCV- and IFN- treated cells and the observed elevation of 2-5A provides direct evidence for the activation of OAS by viral dsRNA and the RNase L involvement in RNA degradation [71]. Increased levels

of resistance to EMCV infection occurred in human glioblastoma T98G cells stably transfected with a human OAS cDNA, which resulted in constitutive OAS production [72]. In other similar studies, transfection of murine cDNAs encoding the 43-kDa OAS into NIH 3T3 cells results in varying levels of constitutive OAS production, as well as greatly increased resistance to EMCV infection [73]. It has been reported that the antiviral effect of IFN-α/β for EMCV was reduced by 250-fold when expression of the SVT2/ZB1 mutant prevented 2-5A-dependent rRNA cleavage [74]. After RNase L was truncated by 89 C-terminal aminoacid residues, its catalytic activity was completely absent in stably expressed murine SVT2 cells and it resulted in inhibition of the 2-5A system. A number of studies have found an increase of 2-5A levels, activation of RNase L and characteristic rRNA breakdown in vaccine-virus infected, IFN-treated cells [75].

The induction of an antiviral state by type I IFNs was evaluated in primary trigeminal ganglion cells using herpes simplex virus type 1 (HSV-1). The cells treated with mouse IFN-β showed the greatest resistance to HSV-1 infection. In the cells treated with IFN-α and IFN-β, suppression of HSV-1 replication occurred through an RNase L dependent pathway [76]. Over expressed RNase L by >100-fold compared with levels of the endogenous murine RNase L in 3T3/pLZ suppressed the replication of diverse viruses: EMCV, vesicular stomatitis virus, human parainfluenza virus-3, and vaccinia virus. Additional reductions in viral growth were obtained by treating

3T3/pLZ cells with IFN (alpha + beta) before infections. These results directly demonstrate the anticellular and antiviral potential of the 2-5A system [77]. The 2-5A system is also active in the cells with HIV infection [78]. The HIV-1 gene product tat causes a dramatic increase in the steady-state levels of HIV-1 long terminal repeat (LTR)-derived mRNAs. The interaction of tat with a region in the HIV LTR called TAR mediates this up-regulation of HIV mRNAs but the TAR RNA sequence activates OAS [79]. The expression of vector containing OAS that was introduced into coding region downstream of a 3'-LTR of HIV-1 was activated by the HIV tat protein. Apparently through the tat-mediated trans-activation of OAS, resulting in an increase of 2-5A oligonucleotides, the replication of HIV was inhibited in cells transfected with the vector. It has been [80] postulated that HIV-trans–activated OAS could block HIV replication, leading to design a possible therapeutic approach that may be used to treat AIDS. To determine the involvement of RNase L in the control of human immunodeficiency virus type 1 (HIV-1) replication, a segment of the HIV-1 nef gene was replaced with human RNase L cDNA. HIV-1 provirus containing sense orientation RNase L cDNA increased expression of RNase L, resulting in 500- to 1000-folds inhibition of virus replication in Jurkat cells for about 2 weeks [81]. Subsequently, a partial deletion of the RNase L cDNA resulted in an increase of virus production. The anti-HIV activity of RNase L correlated with a decrease of HIV-1 RNA along with acceleration in cell death accompanied by DNA fragmentation. The findings demonstrate that RNase L impairs HIV replication.

B.4 The potential role of RNase l in the immune system

RNase L is present at constitutive basal levels in most mammalian cells and is induced by IFNs, especially in mouse cells [57]. There are remarkable differences of RNase L levels in different tissues. High levels of RNase L expression were found in the spleen and the thymus, which implicates that the enzyme may play a role in the immune system. Mice with targeted disruption of RNase L have enlarged thymuses containing excess numbers of thymocytes, implicating that RNase L may be involved in T-cell development [35]. Furthermore, the immune response to DNA-based vaccine [82] and suppression of skin allograft rejection are impaired in RNase L null mice [83], suggesting that RNase L plays a role in immune responses. It has been reported [84] that RNase L is involved in activation of p-38 MAPK and JNK by dsRNA and EMCV. The consequence of the activation of these pathways is the production of pro-inflammatory and pyrogenic cytokines, such as IL-1β, IL-6, TNF-α, and INF-γ which promotes immune responses.

B.5 RNase L is a tumor suppressor

Over-expression of RNase L in NIH 3T3 cells markedly enhances the antiproliferative function of IFN, whereas the dominant-negative RNase L suppresses the anti-proliferative activity of IFN in SVT2 cells [74]. The 2-5 A/RNase L system contributes to apoptosis of viral infected cells by both degrading cellular RNA and

blocking anti-apoptotic proteins such as Bcl-2 [75]. Proapoptotic function of RNase L may limit some diseases such as prostate cancer. Several studies linked the hereditary prostate cancer 1 (HPC1) allele to the RNase L gene [85,86,87] located at chromosome 1q25, a region deleted or rearranged in some breast cancers. The studies suggest that mutations in RNASEL predispose men to an increased incidence of prostate cancer. The RNase activities of missense variants of human RNase L were compared after expression in a mouse RNase L -/- cell line. Several variants (G59S, I97L, I220V, 322F, Y529C, and D541E) produced similar levels of RNase L activity as a wild-type enzyme, but the R462Q variant, previously implicated in up to 13% of unselected prostate cancer cases, bound 2- 5A at wild-type levels but had a 3-folds decrease in RNase L activity. The deficiency in RNase L (R462Q) activity was correlated with a reduction in its ability to dimerize into a catalytically active form. Furthermore, the RNase L mutant (R462Q) was defective in causing apoptosis in response to 2-5A consistent with its possible role in prostate cancer development. It has been proposed [89] that RNase L functions as a tumor suppressor on the basis of its ability to degrade RNA, thus initiating a cellular stress response that leads to apoptosis. The anti-tumor activity of RNase L can be induced by a small molecule, 2-5A. Indeed, 2-5A activation of RNase L produces a remarkable stimulation of transcription (>/=20-fold) for genes that suppress virus replication and prostate cancer [88]. Among the 2-5A-induced genes are several IFN-stimulated genes, including IFN-inducible transcript 1/P56, IFN-inducible transcript 2/P54, IL-8, and IFN-stimulated gene 15. 2-5A also potently elevated the expression of macrophage inhibitory

cytokine-1/nonsteroidal antiinflammatory drug-activated gene-1, a TGF-beta superfamily member implicated as an apoptotic suppressor of prostate cancer. Transcriptional signaling to the macrophage inhibitory cytokine-1/nonsteroidal anti-inflammatory drug-activated gene-1 promoter was deficient in HeLa cells expressing a nuclease-dead mutant of RNase L, which was JNK and ERK dependent, and both were activated in response to 2-5A treatment. These findings suggest that activation of RNase L by 2-5A may produce antitumor response as demonstrated in a mouse model of prostate cancer [89]. 2-5A also induces apoptosis in prostate cancer cells. The androgen receptor and RNase L interact in a ligand dependent manner, which may be associated with prostate cancer initiation and progression [90]. Furthermore, overexpression of wild type RNase L conferred IFN sensitivity to a dihydrotestosterone inducible reporter gene, whereas R462Q-mutated RNase L is unable. It is suggested that RNASEL variants Glu265X and Arg462Gln might contribute to the tumorigenesis of sporadic and familial pancreatic cancer [91].

B.6 RNase L plays a role in the regulation of gene expression

Documented evidence has shown that RNase L plays an important role in the regulation of the stability of several gene products such as ISG43, ISG15 [92], PKR [93], MyoD mRNA in myocytes [94] and mitochondrial mRNAs in H9 lymphocytes [95]. ISG43 expression was negatively regulated by RNase L in IFN-treated cells. ISG43 induction is a primary response to IFN treatment and requires a functional JAK/STAT

signaling pathway. The kinetics of ISG43 induction was identical in wild type and RNase L-knockout fibroblasts; however, the decline in ISG43 mRNA following IFN treatment was markedly attenuated in RNase L-knockout fibroblasts. The delayed shut-off kinetics of ISG43 mRNA corresponded to an increase in its half-life in RNase L-deficient cells. ISG15 mRNA also displayed RNase L-dependent regulation. These findings show a novel role for the 2-5A system in the attenuation of the IFN response [92].

The role of RNase L in the transient control of the IFN response was also suggested [96]. Khalid et al. found that ectopic expression of RNase L prevented the IFN induction of PKR. After RNase L-null cells were treated with IFN-α, PKR induction was increased and PKR mRNA stability was enhanced as well. In addition, the phosphorylated form of eIF2α appeared with extended kinetics compared with that in similarly treated wild type cells. An enhanced IFN response in RNase L-null cells was also demonstrated by monitoring inhibition of viral protein synthesis. The role of RNase L and RLI in muscle differentiation was determined by transfection of C2 mouse myoblasts with sense and antisense RLI cDNA constructs [94]. Importantly, the over expression of RLI in C2 cells was able to inhibit RNase L activity, as a result, an increased level of MyoD mRNA was observed, leading to accelerate kinetics of muscle differentiation. Inversely, transfection of an RLI antisense construct resulted in increased RNase L activity, reduced MyoD mRNA production, and delayed

differentiation. Consistent with these observations, MyoD mRNA levels were also decreased in C2 cells transfected with an inducible RNase L construct. Therefore, these data suggest that RNase L is directly involved in myoblast differentiation, probably through its role in regulating MyoD stability. In addition, RNase L in also found to interact with eRF3/GSPT1, a human translation termination factor, to regulate the expression of a gene at its translational level [97].

1.4C 2’-5’-phosphodiesterase

2’-5’-phosphodiesterase (2’-PDE) is the third enzyme of the 2-5A system. The recombinant human 2'-PDE expressed in mammalian cells cleaves the 2'-5’ phosphodiester bond of 2-5A analogs, leading to destruction of 2-5A in the cells [98]. No sequences with high homology to this human 2'-PDE are found, so it is considered to be a unique enzyme without isoforms. Suppression of 2'-PDE by a small interfering RNA and a 2'-PDE inhibitor resulted in significant reduction of viral replication, whereas overexpression of 2'-PDE protected cells from IFN-induced antiproliferative activity. These observations identify 2'-PDE as a key regulator of the 2-5A system and as a potential novel target for antiviral and antitumor treatments [98]. The activity of the 2'-5' phosphodiesterase is very high in quiescent cells while the levels of OAS and RNase L are high at the end of S phase [99].

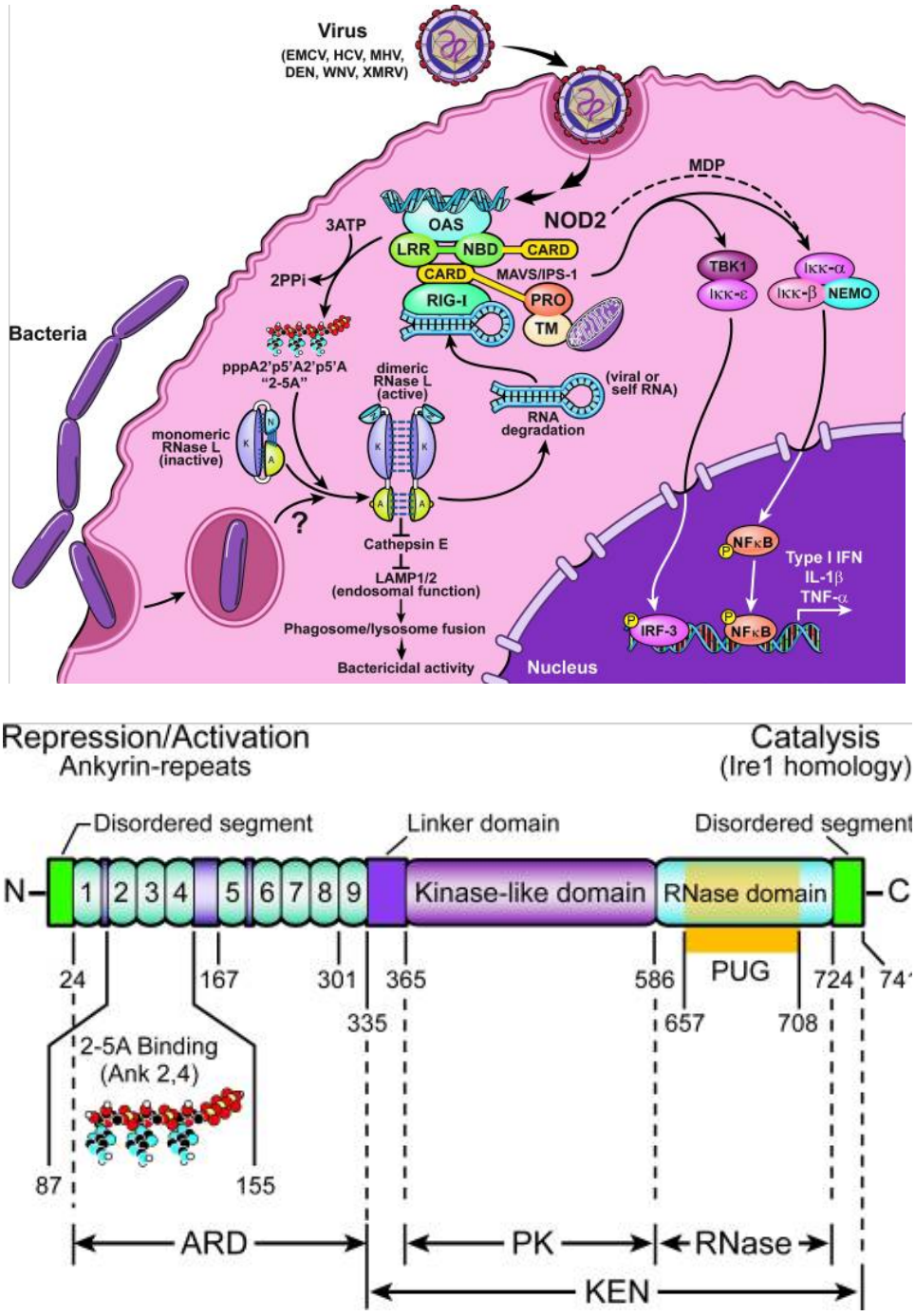

Figure 1-7. The structure of RNase L. (Chakrabarti A, Jha BK, Silverman RH. J Interferon Cytokine Res. 2011)

1.5 Our hypothesis

These observations implicate that RNase L may play an important role in the immune system. Indeed, studies have revealed that skin allograft rejection is suppressed in mice lacking RNase L, suggesting the involvement of RNase L in T cell immunity, particularly $CD4^+$ T cell mediated immunity [100]. In addition, alphavirus-based DNA vaccination against a non-mutated tumor-associate self-antigen (tyrosinase-related protein-1, TRP-1) is severely impaired in RNase L null mice, indicating that RNase L plays an important role in host immune system against cancer [101].

In this study, we present evidence showing that RNase L may be involved in the pathogenesis of type I diabetes. RNase L deficient RIP-B7.1 mice significantly delayed the onset of diabetes induced by STZ and poly I:C. Immunohistostaining revealed that the population of infiltrated $CD8^+$ T cells was remarkably reduced in the islets of RNase L deficient mice, implicating RNase L may contribute to type I diabetes onset through mediating the infiltration of immune cells. Furthermore, RNase L regulated the expression of certain proinflammatory genes in the pancreas under the special condition. Our results suggest a novel role of RNase L in the development of type I diabetes.

1.6 References

[1] Asbun J, Villarreal FJ. The pathogenesis of myocardial fibrosis in the setting of diabetic cardiomyopathy, J Am Coll Cardiol. 47(4):693-700, 2006.

[2] Schnell O, The links between diabetes and cardiovascular disease, J Interv Cardiol.18:413-6. 2005.

[3] Russell TA. Diabetic nephropathy in patients with type 1 diabetes mellitus, Nephrol Nurs J. 33(1):15-28; quiz 29-30, 2006.

[4] Cara JF, Chaiken RL. Type 2 diabetes and the metabolic syndrome in children and adolescents, Curr Diab Rep. 6(3):241-50, 2006.

[5] www.cdc.gov/diabetes

[6] Zimmet P, Alberti KG and Shaw J. Global and societal implication of the diabetes epidemic, Nature, 414: 782-787, 2001.

[7] Mathis, et al. β-cell death during progress to diabetes, Nature, 414:792-797, 2001.

[8] Yoon JW and Jun HS, Cellular and molecular pathogenic mechanisms of insulin-dependent diabetes mellitus, Ann N Y Acad Sci. 928:200-11, 2001.

[9] Mandrup-Poulsen T, Apoptotic signal transduction pathways in diabetes, Biochemical Pharmacology, 66:1433-1440, 2003.

[10] Anderson MS, Bluestone JA. The NOD mouse: a model of immune dysregulation. Annu Rev Immunol. 23:447-85, 2005.

[11] Solomon M, Sarvetnick N. The pathogenesis of diabetes in the NOD mouse. Adv Immunol. 84:239-64, 2004.

[12] Coppieters KT, Dotta F, Amirian N, Campbell PD, Kay TW, Atkinson MA, Roep BO, von Herrath MG. Demonstration of islet-autoreactive CD8 T cells in insulitic lesions from recent onset and long-term type 1 diabetes patients. J Exp Med. 209(1):51-60, 2012.

[13] Coppieters KT, von Herrath MG. Viruses and cytotoxic T lymphocytes in type 1 diabetes. Clin Rev Allergy Immunol. 41(2):169-78, 2011.

[14] Bergholdt R, et al., Type 1 database mellitus: an inflammatory disease of the islet, Adv Exp Med Biol. 552:129-53, 2004.

[15] Selmi C, Lleo A, Zuin M, Podda M, Rossaro L, Gershwin ME. Interferon alpha and its contribution to autoimmunity. Curr Opin Investig Drugs. 7(5):451-6, 2006.

[16] Chehadeh W, Weill J, Vantyghem MC, Alm G, Lefèbvre J, Wattré P, Hober D. Increased level of interferon-alpha in blood of patients with insulin-dependent diabetes mellitus: relationship with coxsackievirus B infection. J Infect Dis. 181(6):1929-39, 2000.

[17] Stewart TA, Hultgren B, Huang X, Pitts-Meek S, Hully J, MacLachlan NJ, Induction of type I diabetes by interferon-α in transgenic mice, Science, 260:1942-1946, 1993.

[18] Huang X, Hultgren B, Dybdal N, Stewart TA. Islet expression of interferon-alpha precedes diabetes in both the BB rat and streptozotocin-treated mice. Immunity. 1(6):469-78, 1994.

[19] Devendra D, Jasinski J, Melanitou E, Nakayama M, Li M, Hensley B, Paronen J, Moriyama H, Miao D, Eisenbarth GS, Liu E, Interferon-α as a mediator of polyinosinic:polycytidylic acid-induced type 1 diabetes, Diabetes, 54:2549-2556, 2005.

[20] Li Q, Xu B, Michie SA, Rubins KH, Schreriber RD, McDevitt HO. Interferon-alpha initiates type 1 diabetes in nonobese diabetic mice. Proc Natl Acad Sci U S A. 105(34):12439-44, 2008.

[21] M Streuli, S Nagata, C Weissmann. At least three human type alpha interferons: structure of alpha 2, Science, Vol. 209 no. 4463 pp. 1343-1347,1980.

[22] Manuel O. Díaz, et al. Structure of the Human Type-I Interferon Gene Cluster Determined from a YAC Clone Contig. Genomics, 22(3): 540–552, 1994.

[23] Tadatsugu Taniguchi, et al. Human leukocyte and fibroblast interferons are structurally related, Nature, 285, 547 – 549, 1980.

[24] Young HA, Hardy KJ. Role of interferon-gamma in immune cell regulation. J Leukoc Biol.1995;58(4):373–381.

[25] Erika A. Bach, Michel Aguet, and Robert D. Schreiber. THE IFNγ RECEPTOR: A Paradigm for Cytokine Receptor Signaling, Annu. Rev. Immunol, 15:563–91, 1997.

26 S. Pestka, J.A. Langer, K.C. Zoon, C.E. Samuel Annu. Rev. Biochem., 56: 727–777, 1987.

[27] Samuel CE. Antiviral actions of interferons. Clin Microbiol Rev, 14: 778–809, 2001.

[28] Stark GR, Kerr IM, Williams BR, Silverman RH, Schreiber RD. Annu Rev Biochem, 67:227-64, 1998.

[29] Staeheli P, Pitossi F, Pavlovic J. Mx proteins: GTPases with antiviral activity. Trends Cell Biol, 3(8):268-72, 1993.

[30] Haller O, Kochs G. Interferon-induced mx proteins: dynamin-like GTPases with antiviral activity. Traffic, 3(10):710-7, 2002.

[31] Leong JC, Trobridge GD, Kim CH, Johnson M, Simon B. Interferon-inducible Mx proteins in fish. Immunol Rev, 166:349-63, 1998.

[32] Haller O1, Frese M, Kochs G. Mx proteins: mediators of innate resistance to RNA viruses. Rev Sci Tech, 17(1):220-30, 1998.

[33] Kuhen KL1, Shen X, Samuel CE. Mechanism of interferon action sequence of the human interferon-inducible RNA-dependent protein kinase (PKR) deduced from genomic clones. Gene, 178(1-2):191-3, 1996.

[34] Langland JO1, Cameron JM, Heck MC, Jancovich JK, Jacobs BL. Inhibition of PKR by RNA and DNA viruses. Virus Res, 119(1):100-10, 2006.

[35] Zhou A, Paranjape J, Brown TL, Nie H, Naik S, Dong B, Chang A, Trapp B, Fairchild R, Colmenares C, Silverman RH, IFN action and apoptosis are defective in mice devoid of 2',5'-oligoadenylate-dependent RNase L., EMBO J 16(21): 6355-6363, 1997.

[36] Player MR1, Torrence PF. The 2-5A system: modulation of viral and cellular processes through acceleration of RNA degradation. Pharmacol Ther, 78(2):55-113, 1998.

[37] Saarma M, Toots U, Raukas E, Zhelkovsky A, Pivazian A, Neuman T. Nerve growth factor induces changes in (2'-5')oligo(A) synthetase and 2'-phosphodiesterase activities during differentiation of PC12 pheochromocytoma cells. Exp Cell Res, 166(1):229-36, 1986.

[38] Yan C1, Sehgal PB, Tamm I. Signal transduction pathways in the induction of 2', 5'-oligoadenylate synthetase gene expression by interferon alpha/beta. Proc Natl Acad Sci U S A, 86(7):2243-7, 1989.

[39] Xuan Feng, et al. Low expression of interferon-stimulated genes in active multiple sclerosis is linked to subnormal phosphorylation of STAT1. Journal of Neuroimmunology, 129(1–2): 205–215, 2002.

[40] P.L. WITT, et al. Isoforms p69 and p100 of 2’, 5’-Oligoadenylate Synthetase Induced Differentially by Interferons In Vivo and In Vitro. Journal of Interferon Research, 13(1): 17-23, 1993.

[41] Schwartz, E L | Nilson, L A. Activation of 2', 5'-oligoadenylate synthetase activity on induction of HL-60 leukemia cell differentiation. Molecular and Cellular Biology, 9(9):3897-3903, 1989.

[42] Testa U, et al. Effect of endogenous and exogenous interferons on the differentiation of human monocyte cell line U937. Cancer Res. 48(1):82-8, 1988.

[43] Rimoldi D1, Dieffenbach CW, Friedman RM, Samid D. 2', 5'-Oligoadenylate synthetase gene expression in revertants of ras-transformed NIH3T3 fibroblasts. Exp Cell Res, 191(1):76-82, 1990.

[44] Wells V, Mallucci L. Expression of the 2-5A system during the cell cycle. Exp Cell Res, 159(1):27-36, 1985 Jul.

[45] Will&s, B. R. G., SaundeA, M. E.; and Williard, H. F. Somut. Cell Mol. Genet. 12,403-408, 1986.

[46] Besse S, Rebouillat D, et al. Ultrastructural localization of interferon-inducible double-stranded RNA-activated enzymes in human cells. Exp Cell Res, 239(2):379-92, 1998.

[47] Bonnevie-Nielsen V, Martensen PM, Justesen J, Kyvik KO, Kristensen B, Levin K, Beck-Nielsen H, Worsaa A, Dyrberg T, The antiviral 2',5'-oligoadenylate synthetase is persistently activated in type 1 diabetes, Clinical Immunology, 96:11-18, 2000.

[48] Williams, B. R. G. & Kerr, I. M. Nature 276, 88–89, 1976.

[49] Williams BRG, Kerr IM, et al. Synthesis and breakdown of pppA2'p5'A2'p5'A and transient inhibition of protein synthesis in extracts from interferon-treated and control cells. Eur J Biochem 92:455-462.

[50] Cayley P J, Knight M, Kerr I M. Virus-mediated inhibition of the ppp(A2'p)nA system and its prevention by interferon. Biochem Biophys Res Commun, 104:376 - 382, 1982.

[51] Floyd-Smith G. (2'-5') An-dependent endoribonuclease: enzyme levels are regulated by IFN beta, IFN gamma, and cell culture conditions. J Cell Biochem, 38(1):13-21, 1988.

[52] Bayard BA, Gabrion JB. 2', 5'-Oligoadenylate-dependent RNAse located in nuclei: biochemical characterization and subcellular distribution of the nuclease in human and murine cells. Biochem J, 296 (Pt 1):155-60, 1993.

[53] Krause D, Panet A, Arad G, Dieffenbach CW, Silverman RH. Independent regulation of ppp (A2'p)nA-dependent RNase in NIH 3T3, clone 1 cells by growth arrest and interferon treatment. J Biol Chem, 260(16):9501-7, 1985.

[54] Sen GC1, Lengyel P. The interferon system. A bird's eye view of its biochemistry. J Biol Chem, 267(8):5017-20, 1992.

[55] Wang L1, Zhou A, et al. Elevated levels of 2', 5'-linked oligoadenylate-dependent ribonuclease L occur as an early event in colorectal tumorigenesis. Clin Cancer Res,1(11):1421-8, 1995.

[56] Tanaka N1, Nakanishi M, et al. Structural basis for recognition of 2', 5'-linked oligoadenylates by human ribonuclease L. EMBO J, 23(20):3929-38, 2004.

[57] Zhou A, Hassel BA, and Silverman RH. Expression cloning of 2-5A-dependent RNAase: a uniquely regulated mediator of interferon action, Cell, 72(5):753-765, 1993.

[58] Dong B, Silverman RH. 2-5A-dependent RNase molecules dimerize during activation by 2-5A. J Biol Chem, 270(8):4133-7, 1995.

[59] Dong B, Silverman RH. A bipartite model of 2-5A-dependent RNase L. J Biol Chem, 272(35):22236-42, 1997.

[60] Nakanishi M1, Goto Y, Kitade Y. 2-5A induces a conformational change in the ankyrin-repeat domain of RNase L. Proteins, 60(1):131-8, 2005.

[61] Breeden L, Nasmyth K. Cell cycle control of the yeast HO gene: cis- and trans-acting regulators. Cell, 48(3):389-97, 1987.

[62] Aubry F1, Mattéi MG, Barque JP, Galibert F. Chromosomal localization and expression pattern of the RNase L inhibitor gene. FEBS Lett, 26;381(1-2):135-9, 1996.

[63] Bisbal C1, Martinand C, Silhol M, Lebleu B, Salehzada T. Cloning and characterization of a RNAse L inhibitor. A new component of the interferon-regulated 2-5A pathway. J Biol Chem, 270(22):13308-17, 1995.

[64] Bork P, Sander C. A hybrid protein kinase-RNase in an interferon-induced pathway? FEBS Lett , 334(2):149-52, 1993.

[65] Evans RM, Hollenberg SM. Zinc fingers: gilt by association. Cell, Review, 15; 52(1):1-3, 1988.

[66] Nakanishi M1, Yoshimura A, Ishida N, Ueno Y, Kitade Y. Contribution of Tyr712 and Phe716 to the activity of human RNase L. Eur J Biochem ,271(13):2737-44, 2004.

[67] Squire J1, Zhou A, Hassel BA, Nie H, Silverman RH. Localization of the interferon-induced, 2-5A-dependent RNase gene (RNS4) to human chromosome 1q25. Genomics, 1; 19(1):174-5, 1994.

[68] Robert H. Silverman. A Scientific Journey Through the 2-5A/RNase L System. Cytokine Growth Factor Rev, 18(5-6): 381–388, 2007.

[69] Lengyel P. Tumor-suppressor genes: news about the interferon connection. PNAS, 90:5893–5, 1993.

[70] Paul T. Sobol1 and Karen L. Mossman. ICP0 Prevents RNase L-Independent rRNA Cleavage in Herpes Simplex Virus Type 1-Infected Cells. Virol, 80(1): 218–225, 2006.

[71] Silverman RH, Skehel JJ, James TC, Wreschner DH, Kerr IM. rRNA cleavage as an index of ppp(A2'p)nA activity in interferon-treated encephalomyocarditis virus-infected cells. J Virol, 46(3):1051-5, 1983.

[72] Rysiecki G1, Gewert DR, Williams BR. Constitutive expression of a 2', 5'-oligoadenylate synthetase cDNA results in increased antiviral activity and growth suppression. J Interferon Res, 9(6):649-57, 1989.

[73] Li XL, Blackford JA, Hassel BA. RNase L mediates the antiviral effect of interferon through a selective reduction in viral RNA during encephalomyocarditis virus infection. J Virol, 72(4):2752-9, 1998.

[74] Hassel BA, Zhou A, Sotomayor C, Maran A, Silverman RH, A dominant negative mutant of 2-5A-dependent RNase suppresses antiproliferative and antiviral effects of IFN. EMBO J 12: 8, 3297-304, 1993.

[75] Díaz-Guerra M1, Rivas C, Esteban M. Inducible expression of the 2-5A synthetase/RNase L system results in inhibition of vaccinia virus replication. Virology, 227(1):220-8, 1997.

[76] Carr DJ1, Al-khatib K, James CM, Silverman R. Interferon-beta suppresses herpes simplex virus type 1 replication in trigeminal ganglion cells through an RNase L-dependent pathway. J Neuroimmunol, 141(1-2):40-6., 2003

[77] Zhou A, Paranjape JM, et al. Impact of RNase L overexpression on viral and cellular growth and death. JICR, 18(11): 953-61, 1998.

[78] Wu JM1, Chang CC, Chiao JW, Wang CH. 2',5'-Oligoadenylate (2-5A) binding protein (RNase L) changes in AIDS and mammalian cells/tissues. J Exp Pathol, 5(2):79-88, 1990.

[79] Maitra RK1, McMillan NA, Desai S, et al. HIV-1 TAR RNA has an intrinsic ability to activate interferon-inducible enzymes. Virology, 204(2):823-7, 1994.

[80] Schröder HC1, Ugarkovic D, Merz H, et al. Protection of HeLa-T4+ cells against human immunodeficiency virus (HIV) infection after stable transfection with HIV LTR-2',5'-oligoadenylate synthetase hybrid gene. FASEB J, 4(13):3124-30, 1990.

[81] Maitra RK1, Silverman RH. Regulation of human immunodeficiency virus replication by 2',5'-oligoadenylate-dependent RNase L. J Virol, 72(2):1146-52, 1998.

[82] Leitner WW, Hwang LN, et al. Alphavirus-based DNA vaccine breaks immunological tolerance by activating innate antiviral pathways. Nat Med, 9(1):33-9, 2003.

[83] Silverman RH, Zhou A, Auerbach MB, Kish D, Gorbachev A and Fairchild RL , Skin Allograft Rejection is Suppressed in Mice Lacking the Antiviral Enzyme, 2',5'-Oligoadenylate Dependent RNase L, Viral Immunology, 15:77-83, 2002.

[84] Li T1, Zhang J. Stable expression of three genes from a tricistronic retroviral vector containing a picornavirus and 9-nt cellular internal ribosome entry site elements. J Virol Methods, 115(2):137-44, 2004.

[85] Neville PJ1, Conti DV, et al. Prostate cancer aggressiveness locus on chromosome 7q32-q33 identified by linkage and allelic imbalance studies. Neoplasia, 4(5):424-31, 2002.

[86] Wang L1, McDonnell SK, et al. Analysis of the RNASEL gene in familial and sporadic prostate cancer. Am J Hum Genet, 71(1):116-23, 2002.

[87] Rökman A1, Ikonen T, et al. Germline alterations of the RNASEL gene, a candidate HPC1 gene at 1q25, in patients and families with prostate cancer. Am J Hum Genet, 70(5):1299-304, 2002.

[88] Malathi K, Paranjape JM, et al. A transcriptional signaling pathway in the IFN system mediated by 2'-5'-oligoadenylate activation of RNase L. Proc Natl Acad Sci U S A, 102(41):14533-8, 2005.

[89] Xiang Y, Wang Z, et al. Effects of RNase L mutations associated with prostate cancer on apoptosis induced by 2',5'-oligoadenylates. Cancer Res, 63(20):6795-801, 2003.

[90] Bettoun DJ1, Scafonas A, et al. Interaction between the androgen receptor and RNase L mediates a cross-talk between the interferon and androgen signaling pathways. J Biol Chem, 280(47):38898-901,2005.

[91] Bartsch DK1, Fendrich V, et al. RNASEL germline variants are associated with pancreatic cancer. Int J Cancer, 117(5):718-22, 2005.

[92] Li XL, Blackford JA, et al. RNase-L-dependent destabilization of interferon-induced mRNAs. A role for the 2-5A system in attenuation of the interferon response. J Biol Chem, 275(12):8880-8, 2000.

[93] Khabar KS1, Siddiqui YM, et al. RNase L mediates transient control of the interferon response through modulation of the double-stranded RNA-dependent protein kinase PKR. J Biol Chem, 278(22):20124-32, 2003.

[94] Bisbal C1, Silhol M, et al. The 2'-5' oligoadenylate/RNase L/RNase L inhibitor pathway regulates both MyoD mRNA stability and muscle cell differentiation. Mol Cell Biol, 20(14):4959-69, 2000.

[95] Le Roy F1, Bisbal C, et al. The 2-5A/RNase L/RNase L inhibitor (RLI) [correction of (RNI)] pathway regulates mitochondrial mRNAs stability in interferon alpha-treated H9 cells. J Biol Chem, 276(51):48473-82, 2001.

[96] Bahar AM1, Ghalib HW, et al. Maternal serum interleukin-6, interleukin-8, tumor necrosis factor-alpha and interferon-gamma in preterm labor. Acta Obstet Gynecol Scand, 82(6):543-9, 2003.

[97] Le Roy F1, Salehzada T, et al. A newly discovered function for RNase L in regulating translation termination. Nat Struct Mol Biol, 12(6):505-12, 2005.

[98] Kubota K1, Nakahara K, et al. Identification of 2'-phosphodiesterase, which plays a role in the 2-5A system regulated by interferon. J Biol Chem, 279(36):37832-41, 2004.

[99] Wells V, Mallucci L. Expression of the 2-5A system during the cell cycle. Exp Cell Res, 159(1):27-36, 1985.

[100] Silverman RH, Zhou A, Auerbach MB, Kish D, Gorbachev A and Fairchild RL , Skin Allograft Rejection is Suppressed in Mice Lacking the Antiviral Enzyme, 2',5'-Oligoadenylate Dependent RNase L, Viral Immunology, 15:77-83, 2002.

[101] Leitner WW, Hwang LN, DeVeer ML, Zhou A, Silverman RH, Williams BRG, Dubensky TW, Ying H and Nicholas P. Restifo, Alphavirus-based DNA vaccine breaks immunological tolerance by activating innate antiviral pathways" Nature Medicine, 9:33-39, 2003.

PROJECT II:

DEVELOPMENT OF QUANTITATIVE LC-MS/MS METHODS FOR THE PHARMACOLOGICAL STUDIES OF ANTI-CANCER DRUG CANDIDATES

1.7 Overview of 6-hydroximino-4-aza-A-homo-cholest-3-one

The synthesis of some aza-homosteroid compounds with unusual and interesting structures has been reported recently [1-4] (Figure 1-8). These compounds exhibit valuable biological activities such as cytotoxicity and antibacteria. Study of aza-homosteroids indicates that the presence of the characteristic group (-NH-CO-) in the aza-homosteroid molecule has been demonstrated to be important in lowering toxicity and improving anti-tumor activity of the compounds in cancer treatment [5].

It was reported that 6-hydroximino-4-aza-A-homo-cholest-3-one and 6-hydroxyl-4-aza-A-homo-cholest-3-one (Figure 1-9), new steroidal lactams displayed antiproliferative activity against some cancer cells through inducing cancer cell apoptosis by activation of the intrinsic pathway. The apoptotic function of the

compounds was demonstrated by release of cytochrome C, activation of caspase 3 and annexin V labeling**.** Furthermore, the compound was able to inhibit tumor growth in an athymic mouse model. (Table 1-1)

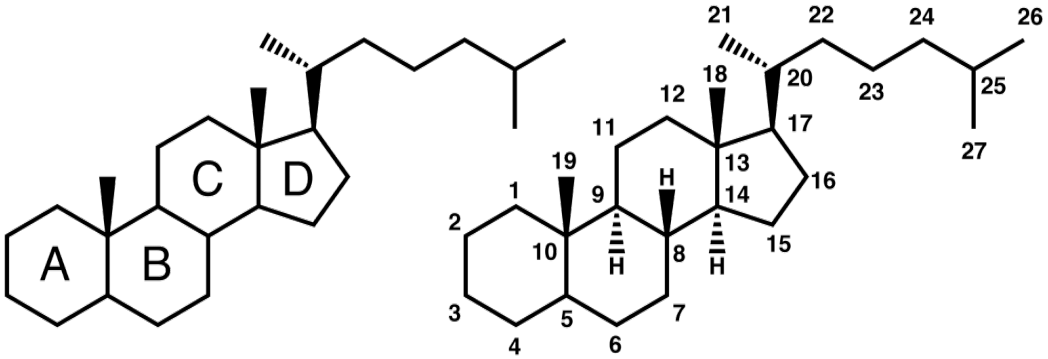

Figure 1-8. Steroidal derivatives

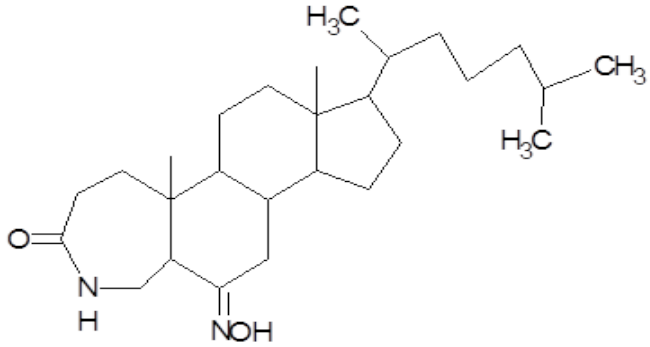

Figure 1-9. The structure of 6-hydroximino-4-aza-A-homo-cholest-3-one

Table 1-1. In vitro anti-tumor activities (IC50 in μmol /L) of the compounds

Compound	Carcinoma Cell Lines				
	GNE 2	SPC-A	Tu 686	PC-3	HT-29
1	12.1	74.5	24.9	14.5	10.6
2	15.8	35.3	31.2	18.3	15.5

1.8 Pharmacological studies of anti-cancer drug candidates

The monitoring of anticancer drugs in biological fluids and tissues is important during both pre-clinical and clinical development and often in routine clinical use. Traditionally, liquid chromatography (LC) in combination with ultraviolet (UV), fluorescence, or electrochemical detection is employed for this purpose. The successful hyphenation of LC and mass spectrometry (MS), however, has dramatically changed this. MS detection provides better sensitivity and selectivity than UV detection and, in addition, is applicable to a significantly larger group of compounds than fluorescence or electrochemical detection. Therefore, LC-MS has now become the method of first choice for the quantitative bioanalysis of many anticancer agents. There are still, however, a lot of new developments to be expected in this area, such as the introduction of more sensitive and robust mass spectrometers, high-throughput analyses, and further optimization of the coupled LC systems. Many articles have appeared in this field in recent years. In this study, we use LC-MS as a powerful tool for the quantitative analysis of anticancer drugs in biological samples.

The efficacy and toxicity of many anticancer drugs are related to parent drug and/or metabolite concentrations in body fluids and tissues. Therefore, during both pre-clinical and clinical drug development, profound knowledge of the pharmacokinetic properties (absorption-distribution-metabolism-elimination; ADME) of the drug is essential. Furthermore, since anticancer agents often have narrow

therapeutic ranges and inter-and intra-patient variability in pharmacokinetic properties are high, drug monitoring in routine clinical use may be required for safe and efficacious therapeutic use [1]. Traditionally, liquid chromatography (LC) has been employed for this purpose. Since most anticancer agents are non-volatile, thermolabile, and polar compounds, they are usually not amendable to gas chromatography (GC). LC-detection involves predominantly ultraviolet (UV), fluorescence, or electrochemical detection. UV detection, however, is not very sensitive and suffers from low specificity, while fluorescence and electrochemical detection, although more sensitive and specific than UV detection, are limited to compounds with fluorescent or electro-active groups or do otherwise require derivatization. Quantitative detection of small molecules by mass spectrometry (MS), off-line LC-MS for qualitative analysis and on-line GC-MS has been common practice for many years. On-line LC-MS for quantitation purposes, on the other hand, was complicated until the introduction of atmospheric pressure ionization (API) techniques (e.g. atmospheric pressure chemical ionization (APCI) and electrospray ionization (ESI)) in the 1980s. In recent years LC-MS interfaces have further improved, mainly because techniques such as ionspray (ISP; pneumatically assisted ESI), turbo-ionspray (TISP; pneumatically assisted ESI with an additional hot drying gas perpendicular to the spray), and heated nebulizer (HN)-APCI (pneumatically assisted APCI) became available that facilitate the evaporation of LC solvents.

1.9 Quantitative LC-MS/MS method development

1.9.1 High Performance Liquid Chromatography (HPLC)

Chromatography is a physico-chemical separation method: a dissolved substance mixture is piped by a mobile phase (gas or liquid stream) through a stationary phase. The separation is based on the different physical and chemical characteristics of the single components in the substance mixture. Today High-performance liquid chromatography is one of the most used analytical separation techniques, because of its sensitivity, its adaptability to accurate quantitative determinations, its suitability for separating non-volatile species or thermally fragile ones, and its widespread applicability to substances that are of interest in industry and science [6].

1.9.2 Chromatographic working principles

The chromatographic separation starts by applying the sample in the column. The different components move depending on the elution method with different velocities through the column and are detected at the end of the column. The result is a chromatogram which shows the peaks of the different components in dependence to the time, when the substances left the column and are detected. The time needed for the way from the injection to the exit of the column is called dead time. Through interactions between the sample components and the stationary phase the elution of the components is slowed down (Figure 1-10), described by the retention time. The

peaks are also characterized by their peak width, full width at half maximum, peak height, and peak area. Under optimal circumstances the peaks are slim and symmetric. But dispersion effects are responsible for peak broadening. So the shape of the peak gives information about the quality of the separation of the column. Peak shapes with variations on the increasing (fronting) or decreasing side (tailing) indicate inhomogeneity or separation problems. Homogeneous peaks should be slim and regular [7].

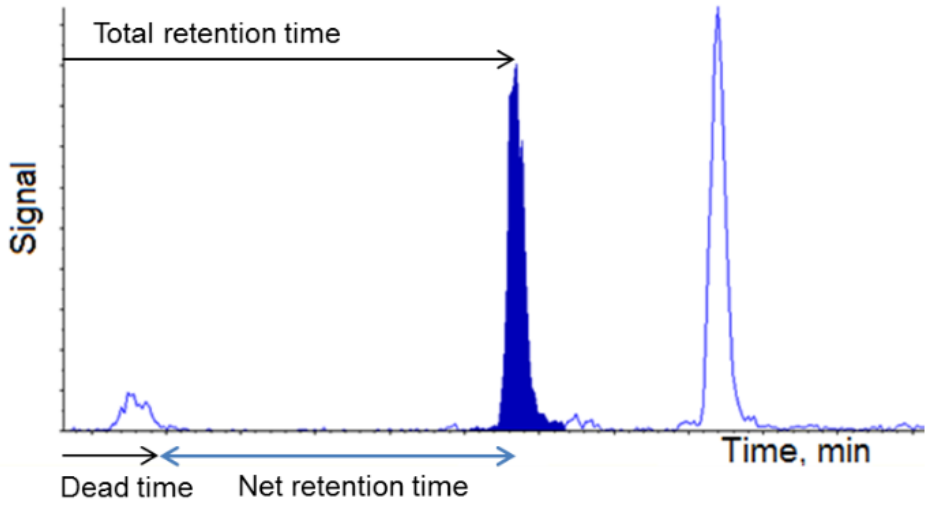

Figure 1-10. Schematic illustration of a chromatogram

"High Performance Liquid Chromatography" is a particular kind of column chromatography. The system consists of a device that pumps the mobile phase, an injector to apply the sample, a column and a detector.

The separation efficiency of the column is dependent on the particle diameter and the pore size of the particles. Due to this separation efficiency the development of HPLC

as separation process is possible. The smaller the particle sizes and the more homogeneously the particle size distribution of the stationary phase in the column, the higher is the separation performance. But the small particle sizes lead to a high packing density of the stationary phase. Now the force of gravity is not enough anymore for the transport of the mobile phase. Therefore the mobile phase has to be pumped through the column with special HPLC pumps. These pumps supply flow rates from 0.1 ¨C 10 mL/min and pressures up to 400 bars.

a. Stationary Phase

Basically, besides silica gel and its modifications, all stationary phases used in column chromatography can be also used in HPLC. In the pharmaceutical sector the most important stationary phase today is the C-18 reversed phase (Table 1-2)

Table 1-2. Stationary Phases used in HPLC

Classification	Stationary phase	Functional groups
Native silica gel	Silica gel	-OH
Polar modified silica gel	Diol phase Cyano propyl phase	-CHOH-CH_2OH -CH_2-CH_2-CH_2-CN
Unpolar modified silica gel (Reversed phase, RP)	C2, C4, C8, C18 Cyclo hexyl phase Phenyl phase Cyano propyl phase	-Alkyl -Cyclo hexyl -Phenyl -CH_2-CH_2-CH_2-CN

b. Mobile Phase

The mobile phase transports the substances through the column. Hydrophilic solvents have a high elution force with polar stationary phases, lipophilic solvents have a high elution force with reversed phases. In the so-called eluotropic row, solvents are classified according to their elution force, for example:

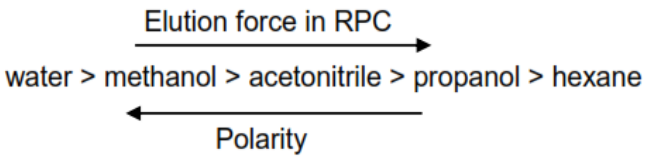

1.9.3 Reversed-phase chromatography (RPC)

In reversed phase chromatography the stationary phase is nonpolar and is called "reversed Phase". The stationary phases are, for example, silica gels modified with lipophilic groups like alkyl-, phenyl- or cyclohexylrests. As mobile phase methanol-water or acetonitrilewater mixtures with appropriate additives (buffer, acids) are often used [4]. The choice of the mobile phase is dependent on the characteristics of the substance, which is examined, and the stationary phase. The elution of substances on a particular stationary phase can be controlled through the composition of the mobile phase. The mobile phases used for HPLC have to be very pure and should be degassed before use. The separation performance of the system is also dependent on the elution velocity. Too small or too high flow rates impair the separation.

1.9.4 Detectors

The substances arrive at the detector after they have passed the separation column. The detection of the substances is an important prerequisite for the proof and the quantification of analyzed components. So the detector should have a high sensitivity for to be determined substances. These detectors are UV/VIS detectors, fluorescence detectors, electrochemical detectors, conductivity detectors and mass selective detectors (mass spectrometry). The interconnection of a HPLC system with a mass spectrometer is the most elaborate detection process in HPLC. The HPLC system is connected with the mass spectrometer by a special interface. The substances separated by HPLC are evaporated and ionized in the interface and brought into the mass spectrometer where they are analyzed [4].

Table 1-3. Typical Chromtographic characteristics for analytical HPLC application [8]

Separation principles	Adsorption - and distribution chromatography, ion pair chromatography, ion change chromatography
Columns	Particles sizes of the column material 3 - 10 µm Column length 10 - 50 cm Column diameter 4 - 10 mm
Mobile phase	Water, acetonitrile, methanol, dichloro-methane, propanol, n-hexane
Mobile phase additives	Mineral acids, acetic acid, aliphatic sulfonic acids, tetrabutylammoniumchloride, buffer, salts
Detectors	UV/VIS detector, fluorescence detector, electrochemical detector, conductivity detector, refraction index detector, HPLC-MS-interconnection

1.10 Mass spectrometry (MS)

Mass spectrometry is an analytical technique used to determine the molecular mass of free ions in a high vacuum. A mass spectrometer is comprised of an ion source, in which gaseous ions are formed, a mass analyzer, which separates the ions with respect to their mass to the charge ratio (m/z) and a detector that measures the ion flow. As a result, a mass spectrum is generated in which the relative frequencies of the ions are plotted against their m/z ratios. The ionization of the analytes can either be made by uptake or loss of an electron or a proton. This is, for instance, reached by bombarding the sample with electrons (electron impact ionization, EI), with atoms or ions (fast atom bombardment (FAB) ionization) or with photons (laser desorption/ionization, LDI). For polar, non-volatile molecules it is possible to do the ionization of the dissolved sample in an electric field (electrospray ionization, ESI) or from the solid phase by means of matrix-assisted laser desorption/ionization (MALDI). For the separation and the detection of analyte ions there are several analyzers with appropriate detectors. The separation of the ions can be effected:

a. By the combination of a magnetic field with an electric field (sector instruments)

b. In the high-frequency field of a quadrupole system (quadrupole instruments)

c. According to their flight time in a test tube in conjunction with a pulsed ion generation (time-of-flight, TOF, instruments).

Ions can also be collected in an electric ion trap (ion trap) or magnetic ion trap (ion

cyclotron resonance cell ICR) followed by mass analysis of characteristic resonance frequencies.

1.10.1 Ion source

The connection of LC and MS is done by means of an ion source. The ion source has not only the task to vaporize and ionize the analyte, but also to remove excessive solvent from the HPLC to keep up the required high vacuum in the MS. In the present work the ionization is done by Electro spray ionization (ESI) (Figure1-11).

Ionization principle:

In the electric field, the ions are transferred into the gas phase at atmospheric pressure.

This process consists of four steps:

a. Formation of small charged droplets of electrolyte solution.

b. Continuous loss of solvent by evaporation of these droplets, whereas the charge density increases at the droplet surface.

c. Repeated spontaneous degradation of the droplets (Coulomb explosion).

d. Desolvation of the analyte at the transfer into the mass spectrometer.

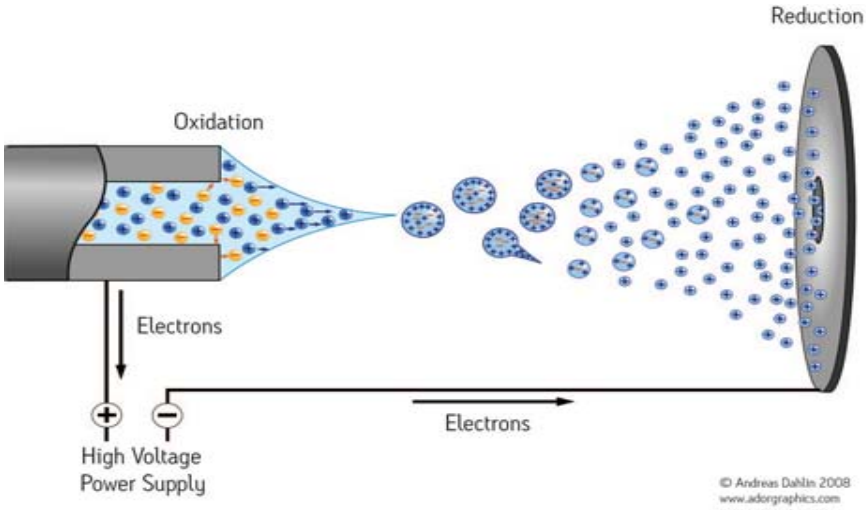

Figure 1-11. Principle of electrospray ionization

The ESI process begins with the continuous supply of dissolved analyte molecules to the tip of a conductive capillary. The applied electric field between the capillary tip and a mass spectrometer also penetrates the analyte solution and separates the ions. For the detection of positively charged ions (positive mode), the positive ions are pulled to the liquid surface. Accordingly, the negative ions are pushed in the opposite direction until the electric field is withdrawn within the liquid through the redistribution of negative and positive ions. The positive ions accumulated at the liquid surface are further drawn towards the cathode. This produces a characteristic liquid cone (Taylor cone), because the surface tension of the liquid counteracts the electric field. In the sufficiently high electric field the cone is stable and is released from the tip, a continuous filament-like liquid flow with a few millimeters in diameter. At some distance from the anode this liquid flow becomes unstable and is divided into tiny droplets. The surface of the droplets is enriched with positive charges. Since there are no negative counter ions anymore, there is a positive net charge. The first formed

droplets have a diameter of a few micrometers and have a high charge density (about 10^5 charges per droplet). These droplets are close to the stability limit (Rayleigh limit) concerning their composition, size and charge. This stability limit is determined by the repulsive Coulomb force of same charges and the cohesive surface tension of the solvent. The Rayleigh equation [9] indicates when the charge Q is equal to the surface tension γ:

$$Q^2 = 64\pi^2 * \varepsilon_0 * \gamma * r^3$$
$$\varepsilon_0: dielectric\ constant\ of\ vakuum$$
$$r: droplet\ radius$$
$$Q: charge$$
$$\gamma: surface\ tension$$

By the evaporation of the solvent and at constant charge Q, the droplets shrink until the radius exceeds the Rayleigh limit. Now the droplets break through the repulsion of the same charges in many small droplets of a few nanometers in diameter (Coulomb explosion). The last step of the ESI process is the evaporation of the rest of the solvent and the transfer of the produced ions into the mass spectrometer [7].

1.10.2 Mass analyzer

The produced ions are analyzed with a mass analyzer. It scans the ions and puts out a mass spectrum, in which the detected masses and the corresponding retention times are shown. The higher the detected peak is, the more ions of the same mass are in the sample. Usually two connected mass analyzers are used to achieve a lower detection

limit and a higher selectivity. Between these two mass analyzers there is a collision chamber in which the mother ions are fragmented into smaller pieces. With this tandem mass spectrometry individual components can be detected specifically within a complex mixture. The most frequently used mass analyzers are the triple quadrupole and the quadrupole ion trap mass analyzers.

1.10.3 Tandem mass spectrometry

With triple quadrupole instruments (Figure 1-12), not only detailed information on the mass but also on the structure of the ions can be obtained. The triple quadrupole mass spectrometer consists of four quadrupoles Q0 to Q3 with two measuring quadrupoles (Q1 and Q3). Q0 is a so-called assistant quadrupole which is operated with alternating current. It focusses the generated ions and transfers them efficiently into the center of the quadrupole field where they begin to oscillate. Q1 is the first measuring quadrupole which scans the ions. Q2 is a collision chamber which can be filled with gas (e.g. nitrogen). By collision with inert gas atoms, the ions coming out from Q1 fragment into Q2. The molecular weights of the resulting fragment ions are then determined in quadrupole Q3. The triple quadrupole mass spectrometer can operate in different modes of measurement.

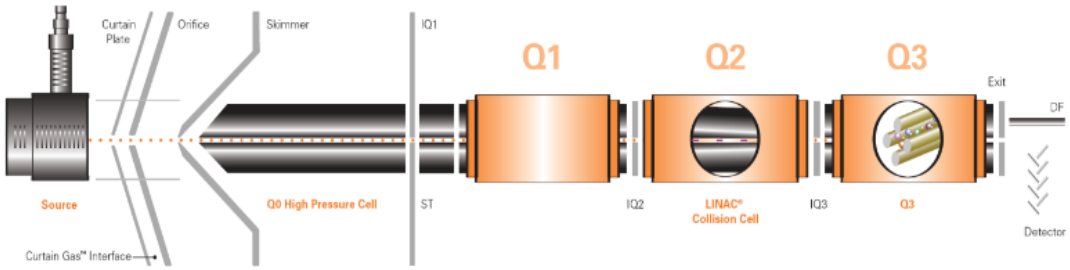

Figure 1-12. Composition of a Triple Quadrupole Mass spectrometer. (Applied Biosystems 2001)

1.11 References

[1] Natalija MK, Mira SB, Željko Ž, Mirjana DP, Zorica DJ, Vladimir DP. Synthesis of some steroidal oximes, lactams, thiolactams and their antitumor activities, Steroids 2007; 72:406–414.

[2] Anna IK, Manolis A, Evagelia SA, Athanasios P, George NP, Sotiris SN. Rational design, synthesis, and in vivo evaluation of the antileukemic activity of six new alkylating steroidal esters, Bioorg. & Med. Chem. 2008; 16:5207–5215.

[3] Dimitrios TPT, George DG, Catherine K, Athanasios P, Panayiotis K, Charalambos C. Lactandrate: A D-homo-aza-androsterone alkylator in the treatment of breat cancer. Breast Cancer Research and Treatment 2006; 97:17–31.

[4] Mohamed EF, Gamal AE, Emad FE, Hanaa MR, Mohamed AT. Novel modified steroid derivatives of androstanolone as chemotherapeutic anti-cancer agents, Europ. J. Med. Chem. 2009; 44:3936–3946.

[5] Catsoulacos P, Catsoulacos D. Antitumor activity of homo-aza-steroidal esters of p-N,N-bis(2-chloroetheryl)amino phenoxy acetic acid, Anticancer Res. 1993;13:1203-1208.

[6] Annesley, T.M., Ion suppression in mass spectrometry. Clin Chem, 2003. 49(7): p. 1041-4.

[7] Gnann, H. Phosphatidylethanol-Ein Alkoholkonsummarker auf dem Weg in die klinisch-forensische Routinediagnostik. 2011. University of Freiburg.

[8] Andreas Dominik, D.S., Instrumentelle Analytik. Second ed, ed. D.A. Verlag.

[9] Honghai Jiang. Nanoelectrospray Mass Spectrometry for Molecular Non-covalent Interactions and proteomics, p22, 2006.

[10] Cui J-G, Gan C-F, Fan L. NMR spectral characteristic and conformation analysis of (3*E*)-cholest-4-en-3,6-dione-3-oxime and (6*E*)-cholest-4-en-3,6-dione-6-oxime. J Instru Anal (*Chinese*), 2008;27:523-526.

[11] Gnann, H., Engelmann, C., Skopp, G., Winkler, M., Auwarter, V., Dresen, S., Ferreiros, N., Wurst, F.M., and Weinmann, W., Identification of 48 homologues of phosphatidylethanol in blood by LC-ESI-MS/MS. Anal Bioanal Chem, 2010. 396(7): p. 2415-23.

[12] Douglas A. Skoog, F.J.H., Stanley R. Crouch, Principles of Instrumental Analysis. Fifth ed. 1998.

[13] Lottspeich, F., Bioanalytik. Second ed. 2006: Elsevier Spektrum akademischer Verlag.

[14] Aradottir, S., Seidl, S., Wurst, F.M., Jonsson, B.A., and Alling, C., Phosphatidylethanol in human organs and blood: a study on autopsy material and influences by storage conditions. Alcohol Clin Exp Res, 2004. 28(11): p. 1718-23.

[15] U.S. Department of Health and Human Services, F.D.A. Guidance for Industry: Bioanalytical Method Validation 2001 [cited 2011 24 September]; Available from: http://www.fda.gov/downloads/Drugs/GuidanceComplianceRegulatoryInformation/Guidances/ucm070107.pdf.

[16] Helander, A., Zheng, Y., Molecular species of the alcohol biomarker phosphatidylethanol in human blood measured by LC-MS. Clin Chem, 2009. 55(7): p. 1395-1405.

[17] Zheng, Y., Beck, O., Helander, A. Method development for routine liquid chromatography-mass spectrometry measurement of the alcohol biomarker phosphatidylethanol (PEth) in blood. Clin Chim Acta, 2011. 412(15-16): p. 1428-1435.

CHAPTER II

INVESTIGATION OF THE CONTRIBUTION OF RNASE L TO THE PATHOGENESIS OF TYPE I DIABETES

2.1 Introduction

In this study, an RNase L deficient RIP-B7.1 mouse line was created which is more vulnerable to environmentally harmful factors such as viral infection. The onset of type I diabetes was found to be significantly delayed in these RNase L deficient RIP-B7.1 mice induced by polyinosinic:polycytidylic acid (poly I:C), a type of double-stranded RNA which is used to mimic viral infection, and Streptozotocin (STZ), a drug which can artificially induce type I-like diabetes in experimental animals. Immunohistostaining showed that the population of infiltrated CD8+ T-cells was remarkably decreased in the islets of RNase L deficient mice after poly I:C treatment, implicating RNase L contributing to type I diabetes onset by regulating immune responses. Furthermore, RNase L was responsible for the expression of

certain proinflammatory genes in the pancreas under the special condition. This project provides new insight into the molecular mechanism leading to β-cells destruction in diabetes.

2.2 Reagents and Methods

2.2.1 Tissue Culture and treatment

NIH 3T3 cells, NIT-1 (ATCC) and mouse embryonic fibroblasts (MEF) were grown in DMEM (Cleveland Clinic, OH) supplemented with 10% fetal bovine serum (PAA Laboratories, MA) and antibiotics in a humidified atmosphere of 5% CO_2 at 37^{o}C. For treatment, NIT-1 cells were grown to 90% confluence and incubated with 1,000 U/ml murine IFN-α (R&D Systems) for 14 h. BMMs were generated from the bone marrow cells of RNase L wild type and deficient C57BL/6 mice by using a modification of a previously reported method [1].

2.2.2 Generation of an RNase L deficient C57BL/6.RIP-B7.1 mouse

An RNase $L^{-/-}$ mouse (C57BL/6) was cross-bred with a C57BL/6.RIP-B7.1 mouse (Barbara Davis Center of Childhood Diabetes, University of Colorado Health Sciences Center, CO). Genotyping for RNase L and B7.1 was performed by using PCR with the condition: denaturing at 96^{o}C for 4 min, for each cycle, denaturing at 96^{o}C for 45 sec, annealing at 55^{o}C for 45 sec, and extension at 72^{o}C for 1.5 min, for 32 cycles, then an additional cycle at 72^{o}C for 5 min. The pair of RNase L primers was: 5'GCA TTG AGG ACC ATG GAG AC3' and 5'GGA GGA GAA GCT TTA

CAA GGT3'; for B7.1, the primers were: TGA AGC CAT GGG CCA CAC3' and 5' GGC TCC TTG TCG GCG TTC TA3'.

2.2.3 Diabetes induction

Six-week-old C57BL/6 RNase L deficient RIP-B7.1 and C57BL/6 RIP-B7.1 wild type mice were injected intraperitoneally (i.p.) with poly I:C (Sigma, St. Louis, MO) daily at a concentration of 5 μg/g body weight for 7 days, and then immunized (i.p.)with 25 μg/mouse for insulin (Eli Lilly, Indianapolis, IN) on day 14 after poly I:C treatment. Blood glucose was measured weekly with the Glucose Oxidase Reagent Set (Pointe Scientific, Canton, MI). Briefly, 10 μl of plasma was mixed with 1ml of the working reagent provided by the manufacturer and incubated at 37^{o}C for exactly 5 min. After incubation, the absorbance at 500 nm were read and recorded. The mice were considered diabetic after two consecutive blood glucose values ≥250 mg/dl.

2.2.4 Immunohistostaining

The pancreas obtained from the mice was fixed in 10% formalin, paraffin embedded and sectioned at 5μm, subsequently stained with hematoxylin and eosin. Pancreatic sections were microscopically examined for infiltration of immune cells. The tissue sections were stained with rat polyclonal antibodies against CD4, CD8, F4/80, CD11b (eBioscience, San Diego, CA) and a monoclonal antibody to insulin (Abcam,

Cambridge, MA), followed by incubating with a peroxidase anti-peroxidase antibody (ICN, Costa Mesa, CA). Images were developed by using 3-3'-diaminobenzidine as a chromogen (Dako, Carpinteria, CA).

2.2.5 Flow Cytometry

Single cell suspension from the spleens was stained with conjugated mAbs including FITC-CD4, PE-CD8, FITC-IgD, PE-B220, APC-Gr.1, FITC-CD11b (BD Pharmingen, San Jose, CA). Cell-associated fluorescence was analyzed with a FACScan instrument and associated Winlist 5 software.

2.2.6 Western blot analysis

After treatment, cells were washed twice with ice-cold PBS and collected with a scraper. The cytoplasmic extracts were prepared by suspension of the cell pellets in the NP-40 lysis buffer (10 mM Tris-HCl, pH8.0, 5 mM $Mg(OAc)_2$, 90 mM KCl, 0.2 mM PMSF, 100 units/ml aprotinin, 10 μg/ml leupeptin and 2% NP-40). After centrifugation at 10,000 x g in a microcentrifuge at 4^oC for 10 min, the cell extracts (100 μg per sample) were fractionated on SDS-10% polyacrylamide gels and transferred to PVDF membranes (Millipore, Billerica, MA). The membranes were blocked with 5% nonfat milk in PBS containing 0.02% sodium azide and 0.2% (v/v) Tween 20, and incubated with different primary antibodies for 1 h at room

temperature. The membranes were then washed with PBS containing 0.2% (v/v) Tween 20 and incubated with specific secondary antibodies conjugated with horseradish peroxidase (Cell Signaling**,** Billerica, MA) for 1 h at room temperature. After washing, the proteins were detected by a chemiluminescent method according to the manufacturer's specification (Pierce, Rockford, IL). Pancreatic tissue extracts obtained from mice (2/group) treated with or without poly I:C (Sigma, St. Louis, MO) every other day at a concentration of 5 μg/g body weight for one week (three times) were analyzed as described above.

2.2.7 Enzyme-linked immunosorbent assay (ELISA)

The expressing level of proinflammatory genes in the extracts of the pancreases was measured by ELISA with commercial available kits (eBioscience, San Diego, CA and R&D Systems, Minneapolis, MN). Briefly, flat bottom 96-well ELISA plates were coated with a capture antibody at 4°C according to manufacturer's instruction. After overnight incubation at 4°C, the plates were washed three times and blocked with the blocking buffer provided in the kit, and then incubated with standards and cell culture medium samples for 2 h at room temperature. After washing the plates, a specific biotinylated antibody was added to each well and incubated for 1 h, followed by washing and 30 min incubation with avidin peroxidase. Then, substrates containing 3, 3' 5, 5'-tetramethylbenzidine (TMB) and hydrogen peroxide were added, and the reaction was terminated by adding 50 μl of phosphoric acid after 30min. Plates were

read at 450nm in a 96-well LD 400C microplate reader (Beckman Coulter, Fullerton, CA).

2.3 Results

2.3.1 IFN-α and poly I:C induced the expression of RNase L in the tissues and cells

RNase L is expressed in nearly all types of mammalian cells from mouse to man [23]. To examine the expressing level of RNase L in the pancreas, the tissue extracts of eight different organs from a C57BL/6 mouse (Jackson Laboratory) were analyzed by the 2-5A binding assay [30]. As shown in Figure 2-1A, there are remarkable tissue differences in RNase L levels. High levels of RNase L expression were found in the lung, spleen and thymus. However, the basic level of RNase L in the pancreas was very low. Similar to our previous result, RNase L was found to be highly expressed in primary immune cells (Figure 2-1B). This observation implicates a possible role of RNase L in the immune system. To determine if IFN-α is able to induce the expression of RNase L in pancreatic cells, NIT cells, a murine β-cell line, were treated with IFN-α and the induction of RNase L was examined by Western blot analysis. Obviously, the expression of RNase L was highly inducible in β-cells (Figure 2-1C). Double stranded RNA such as poly I:C can be used to mimic viral infection *in vitro* and *in vivo*.

To determine if poly I:C is able to induce the up-regulation of RNase L expression in the pancreas, mice were treated with or without poly I:C and the expression of RNase L in the pancreatic tissue extracts was measured. Clearly, poly I:C was a potent inducer of RNase L expression in the pancreas (Figure 2-1D).

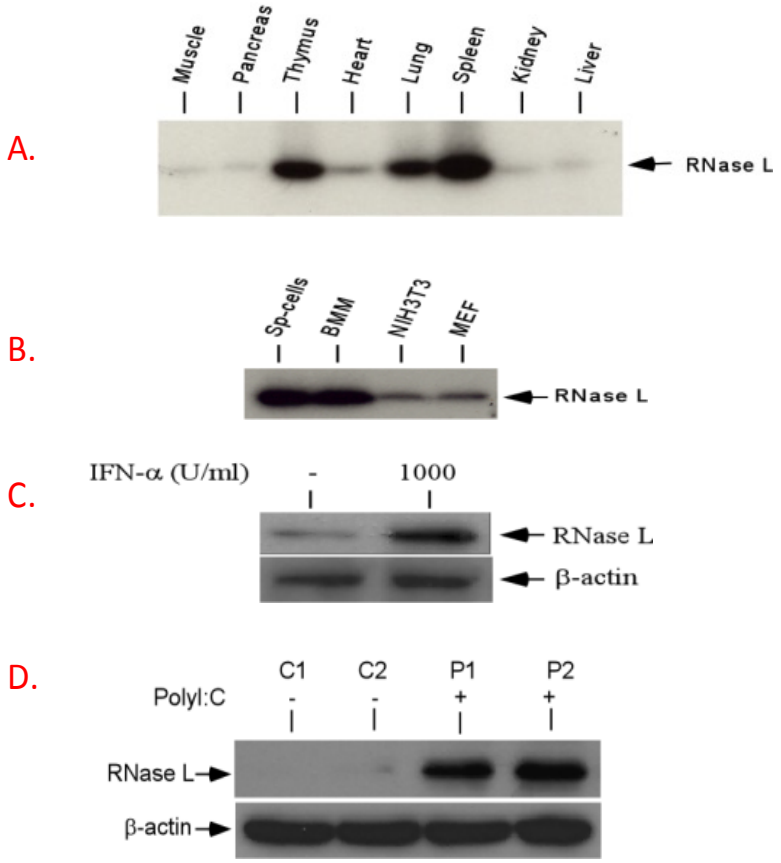

Figure 2-1. The expressing levels of RNase L in the tissue extracts from eight organs (A) and immune cells (B). Sp-cells: primary splenocytes; BMM: bone marrow-derived macrophages; NIH3T3: mouse fibroblasts; MEF: mouse embryonic fibroblasts. (C) IFN-α induces the expression of RNase L in NIT-1 cells. NIT-1 cells were treated with 1,000 units/ml of IFN-α for 16 h and RNase L in the cells was determined by Western blot analysis. (D) Mice (2/group) treated with or without poly I:C at a concentration of 5 μg/g body weight every other days for one week (three

times) and the level of RNase L in the pancreatic tissue extract was determined by Western blot analysis with a polyclonal antibody to mouse RNase L.

2.3.2 RNase L is associated with subclasses of immune cells in the spleen

Splenic cells, in particular B cells, play an important role in autoimmune diseases such as systemic lupus erythematosus (SLE) and type I diabetes. To determine if deficiency of RNase L impacts the subclasses of immune cells in the spleen, splenic cells isolated from RNase $L^{+/+}$ and $^{-/-}$ mice treated with or without either LPS or Poly I:C were subjected to flow cytometry sorting based on cell surface markers. As shown in Figure 2-2A, the population of $CD4^+/CD8^+$ T cells in the spleen of RNase $L^{-/-}$ mice was 37% less than that in the spleen of RNase $L^{+/+}$ mice, whereas the population of the double labeled T cells was 72% less in the spleen of RNase $L^{-/-}$ mice compared to that in RNase $L^{+/+}$ mice after treatment with LPS. Similar to $CD4^+/CD8^+$ T cells, the population of $B220^+$/Ig D^+ B cells in the spleen of RNase L $^{-/-}$ mice was 39% less than that in the spleen of RNase $L^{+/+}$ mice after LPS stimulation although the population of $B220^+$/Ig D^+ B cells in the spleen of intact RNase $L^{-/-}$ mice was slight higher than that in the spleen of RNase $L^{+/+}$ mice under the same condition. In contrast, the population of $Gr.1^+/CD11b^+$ macrophages was almost doubled in the spleen of RNase $L^{-/-}$ mice in compared to that in RNase L $^{+/+}$ mice in the presence of LPS although the ratio of these cell population in both type of untreated mice was nearly equal. Interestingly, Poly I:C treatment increased the population of double labeled

$CD4^+/CD8^+$ T cells by 46% in RNase L wild type mice, but no significant change in the RNase $L^{-/-}$ mice. Similar to LPS treatment, the population of $B220^+/Ig\ D^+$ was decreased by 45% after Poly I:C treatment in RNase $L^{-/-}$ mice whereas the double labeled cells in Poly I:C treated RNase $L^{+/+}$ mice were only slightly more than that in untreated mice. However, the differential change of $Gr.1^+/CD11b^+$ cells after Poly I:C treatment were very close although the percentile of the double labeled cells were significantly increased compared to that in both types of intact mice. Taken together, the results implicate that RNase L may be associated with developing the subclasses of immune cells in the spleen.

A-1.

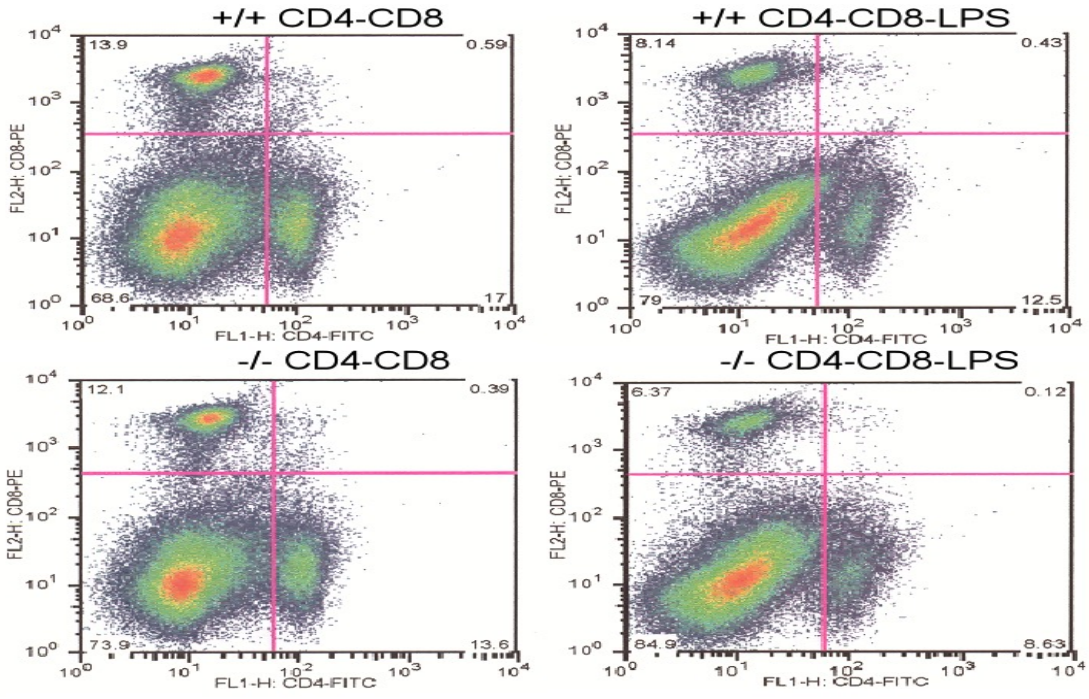

A-2.

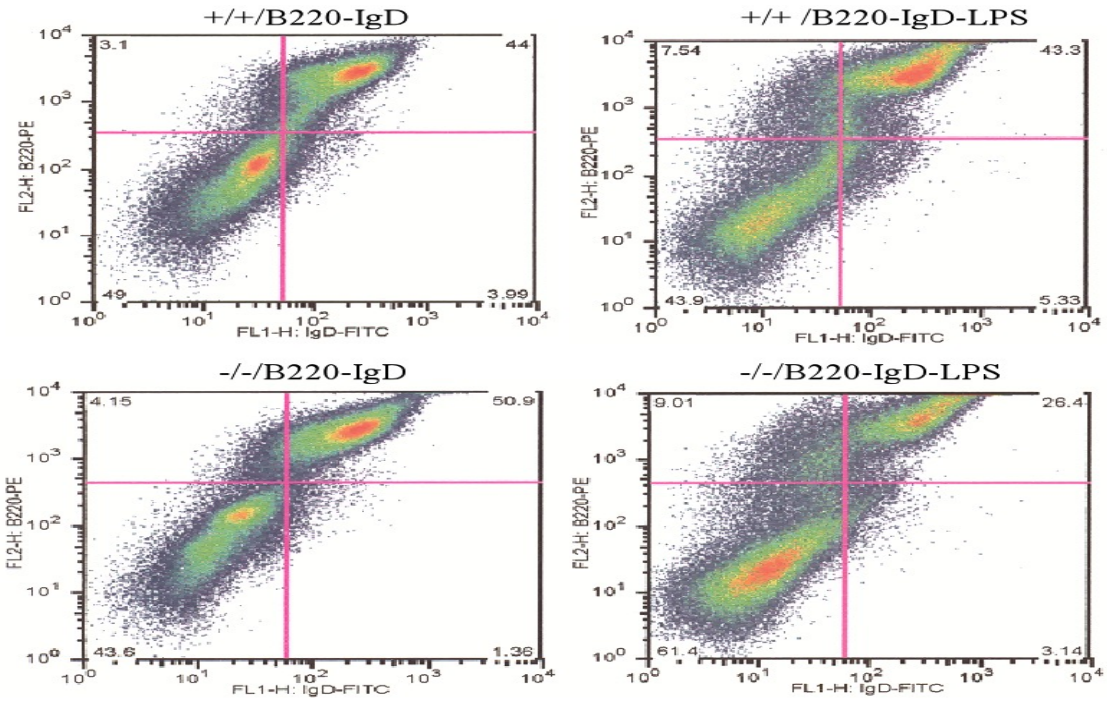
+/+/B220-IgD
3.1
44
49
3.99
+/+ /B220-IgD-LPS
7.54
43.3
43.9
5.33
-/-/B220-IgD
4.15
50.9
43.6
1.36
-/-/B220-IgD-LPS
9.01
26.4
61.4
3.14
FL2-H: B220-PE
FL1-H: IgD-FITC

A-3.

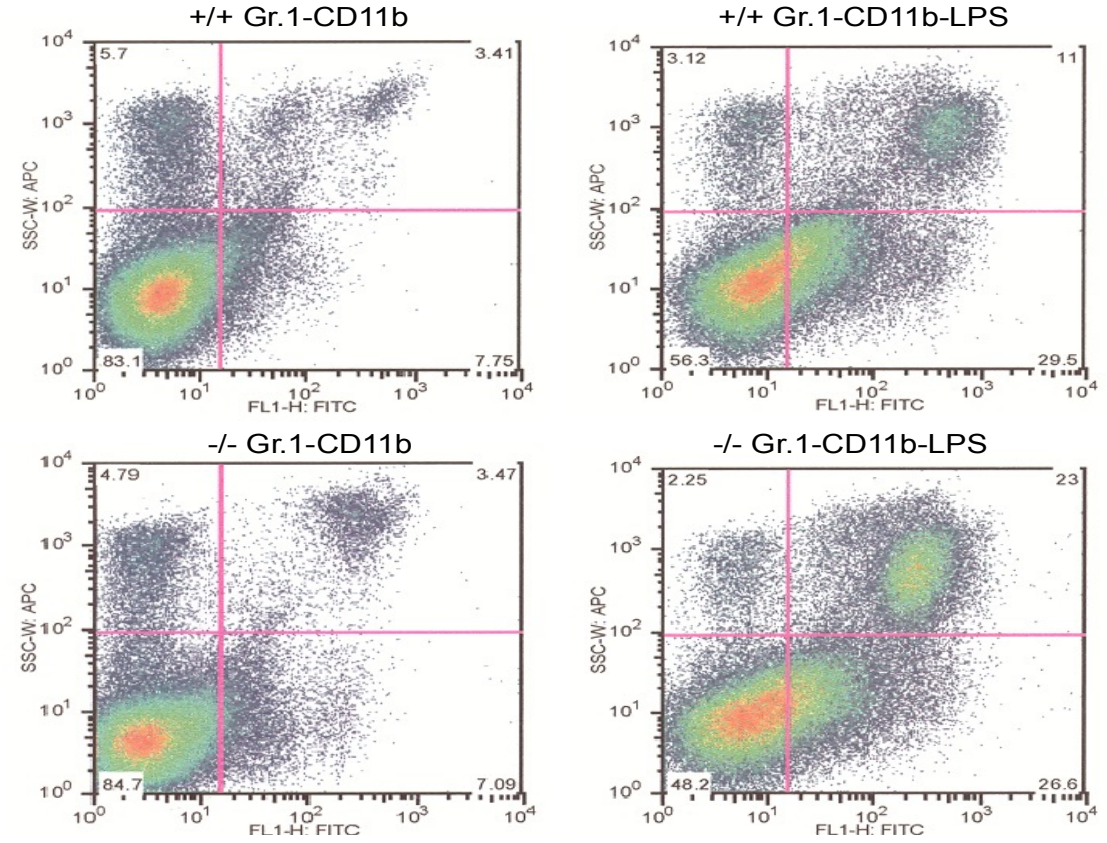
+/+ Gr.1-CD11b
5.7
3.41
83.1
7.75
+/+ Gr.1-CD11b-LPS
3.12
11
56.3
29.5
-/- Gr.1-CD11b
4.79
3.47
84.7
7.09
-/- Gr.1-CD11b-LPS
2.25
23
48.2
26.6
SSC-W: APC
FL1-H: FITC

B-1.

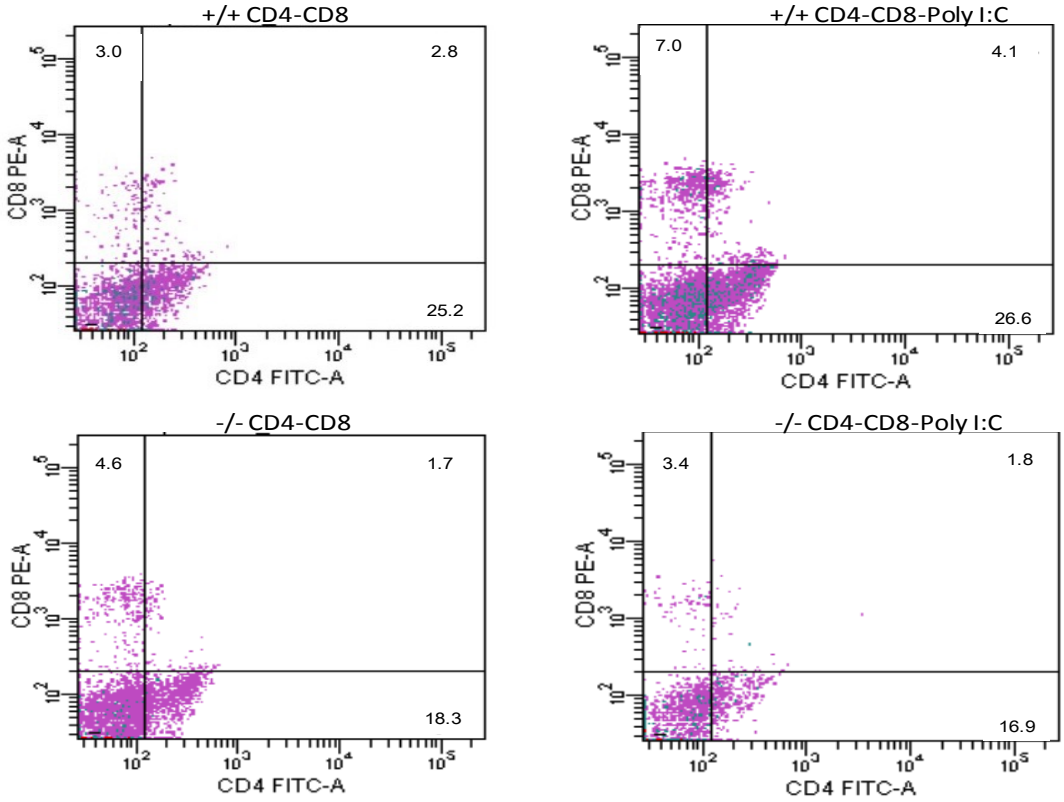
+/+ CD4-CD8
3.0
2.8
25.2
CD8 PE-A
CD4 FITC-A
+/+ CD4-CD8-Poly I:C
7.0
4.1
26.6
CD8 PE-A
CD4 FITC-A
-/- CD4-CD8
4.6
1.7
18.3
CD8 PE-A
CD4 FITC-A
-/- CD4-CD8-Poly I:C
3.4
1.8
16.9
CD8 PE-A
CD4 FITC-A

B-2.

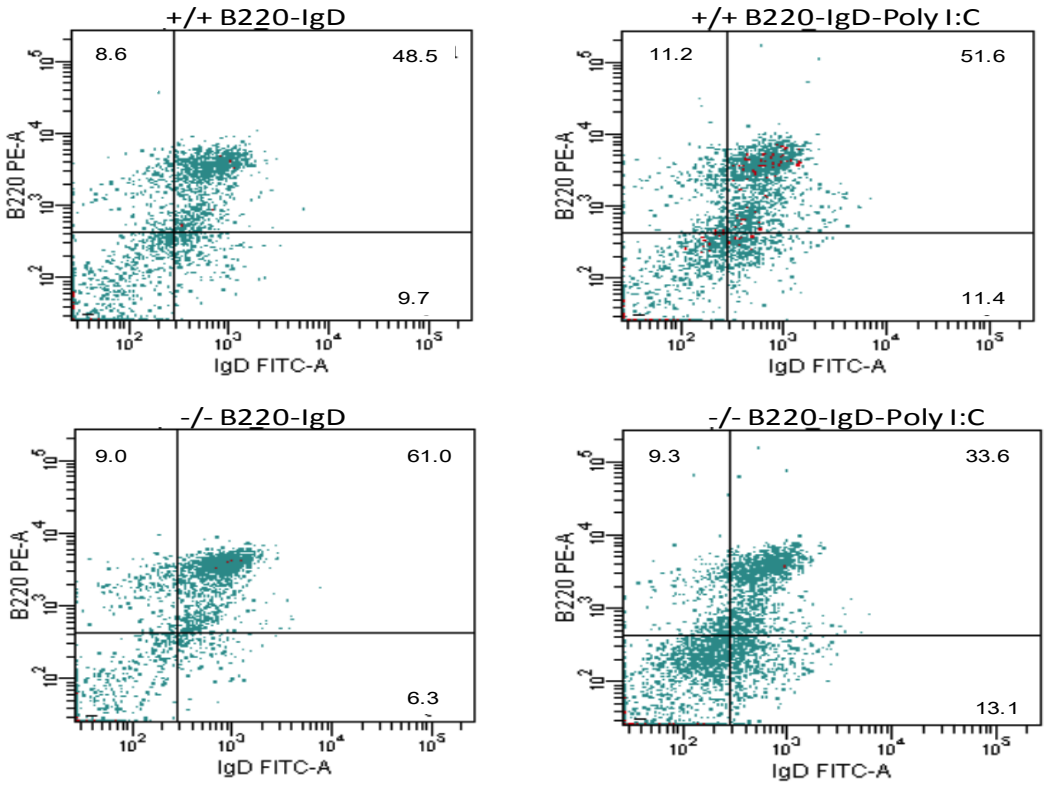
+/+ B220-IgD
8.6
48.5
9.7
B220 PE-A
IgD FITC-A
+/+ B220-IgD-Poly I:C
11.2
51.6
11.4
B220 PE-A
IgD FITC-A
-/- B220-IgD
9.0
61.0
6.3
B220 PE-A
IgD FITC-A
-/- B220-IgD-Poly I:C
9.3
33.6
13.1
B220 PE-A
IgD FITC-A

B-3.

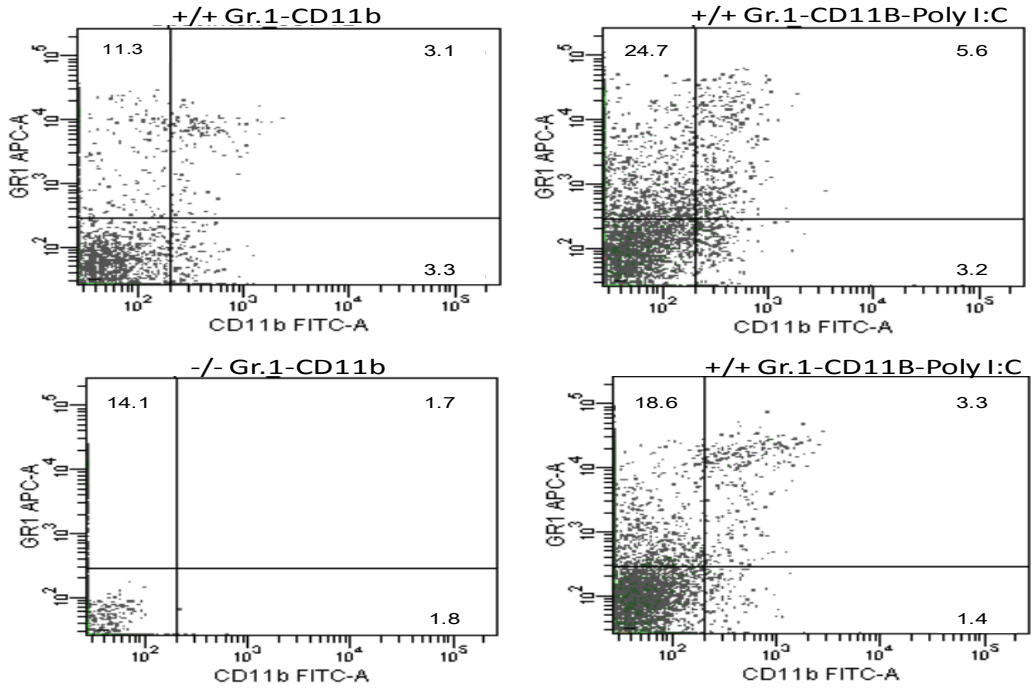

Figure 2-2. Population of immune cells in the spleen Six-week-old male RNase L deficient and wild type mice (3mice/group) were treated with or without 25 μg LPS or 5 μg/g body weight poly I:C for each mouse every other day for a week. The splenic cells combined from three mice were subjected to cell sorting after labeled with CD4, CD8, B220, Ig D, Gr.1 and CD11b alone or combined. A-1 and B-1: CD4/CD8; A-2 and B-2: B220/Ig D; A-3 and B-3: Gr.1/CD11b.

2.3.3 Lack of RNase L delayed the onset of type I diabetes

Viral infection is believed to be a potent factor in triggering autoimmune responses in the pancreas, resulting in destruction of β-cells, leading to absolute deficiency of insulin. Indeed, poly I:C, a type of dsRNA commonly used to mimic viral infection, is

able to effectively induce the onset of type I diabetes in C57BL/6 mice expressing B7.1 on β-cells in the islets under a rat insulin promoter (RIP), which is IFN-α dependent [20]. RNase L can be induced by both poly I:C and IFN-α *in vitro* and *in vivo*, and medicates the functions of IFN-α. To determine the role of RNase L in the onset of type I diabetes induced by poly I:C, RNase L deficient RIP-B7.1 mice were created by cross-breeding an RNase $L^{-/-}$ mouse (C57BL/6) with a C57BL/6.RIP-B7.1 mouse (RIP-B7.1 mouse). The genotype of these mice was determined by PCR as shown in Figure 2-3A. First, the onset of type I diabetes induced by using STZ, a glucose analogue known to induce diabetes in experimental animals, in wild type and RNase L deficient mice was investigated. Mice were interperitoneally (i.p.) injected with 40 mg/kg STZ for five consecutive days, and the blood was collected from the saphenous vein and the level of glucose was measured as described in the Methods. As shown in Figure 2-3B, mice with RIP-B7.1 were more sensitive to STZ-induced diabetic onset and RNase L deficiency markedly delayed the progress of this disease in the RIP-B7.1 mice. To determine if RNase L mediates poly I:C induced onset of type I diabetes, RNase $L^{+/+}$ and $^{-/-}$ RIP-B7.1mice were be injected (i.p.) with 5 μg/g body weight poly I:C daily for 7 days, and then immunized (i.p.) with insulin at 25 μg/mouse on day 14 after poly I:C treatment. Diabetic progress in these mice was monitored every week and the mice were considered diabetic after two consecutive blood glucose values ≥250 mg/dl. As shown in Figure 2-3C, the onset of diabetes was significantly delayed in the RNase L deficient RIP-B7.1 mice.

A.

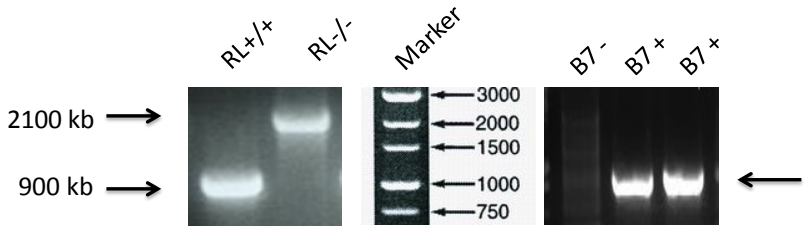

B.

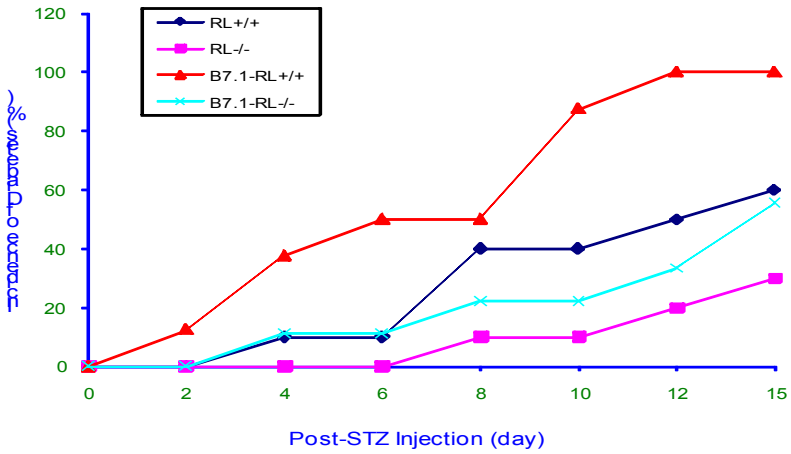

C.

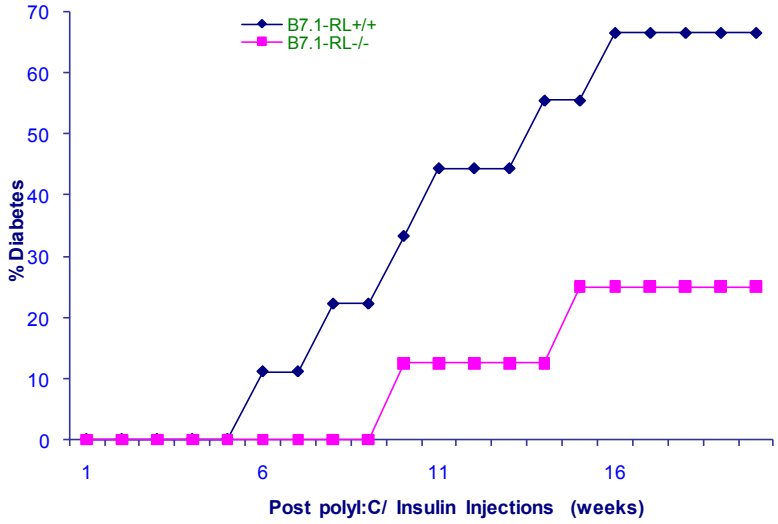

Figure 2-3. Effect of RNase L on STZ and poly I:C-induced diabetes A. Genotyping of B7.1-RL$^{-/-}$ mice. B. Incidence of diabetes in RNase L (RL)$^{+/+}$ and $^{-/-}$ (n=10 for each group), B7.1-RL$^{+/+}$ (n=8) and B7.1-RL$^{-/-}$ (n=9) mice after injection

with 40mg/kg STZ for five consecutive days. C. Incidence of diabetes in B7.1-$RL^{+/+}$ (n=9) and B7.1-$RL^{-/-}$ (n=8) mice after injected (i.p.) with 5 μg/g body weight poly I:C daily for 7 days, and then immunized (i.p.) with 25 μg/mouse of insulin on day 14 after poly I:C treatment. The glucose levels in the blood samples were measured by using a blood sugar test kit (Pointe Scientific). The mice were considered diabetic after two consecutive blood glucose values ≥ 250 mg/dl.

2.3.4 RNase L facilitates infiltration of immune cells

RNase L is highly expressed in the thymus, spleen and all immune cells examined. Since the infiltration of immune cells initiates the progress of this disease, we attempted to investigate if the delay of type I diabetes onset is caused by slowdown of immune responses in the pancreas of mice deficient RNase L. RNase $L^{+/+}$ and $^{-/-}$ RIP-B7.1mice were treated with poly I:C for 40 days. The mice were sacrificed and the pancreatic tissues were embedded and sectioned at 5 μm, subjected to hematoxylin and eosin (H&E) staining. Interestingly, the population of infiltrated immune cells was strikingly reduced in the islets of RNase L deficient mice, suggesting the involvement of RNase L in poly I:C-induced diabetes onset may be through regulating the infiltration of immune cells (Figure 2-4A). To determine the identity of these infiltrated immune cells, immunohistostaining for macrophages, CD4 and CD8 T cells were performed. Apparently, the majority of the infiltrated immune cells in the islets of the pancreas from RNase $L^{+/+}$ mice was CD8 positive T cells

although some of CD4 positive T cells were found in the islets from both types of mice (Figure 2-4B). However, macrophages were undetectable in the islets from both types of mice by using either CD11b or F4/80 as a biomarker (data not shown). The finding indicates that CD8 positive T cells may be the effector cell in the destruction of β-cells in the islets of the pancreas from RNase $L^{+/+}$ RIP-B7.1 mice after poly I:C treatment.

A.

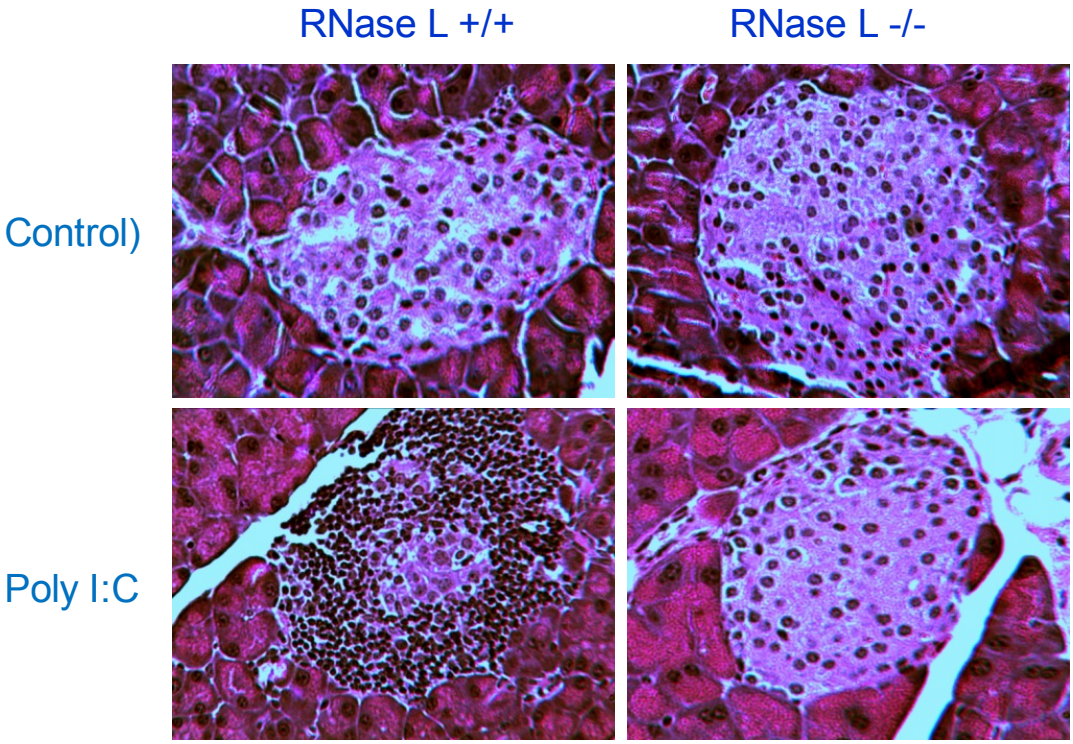

B.

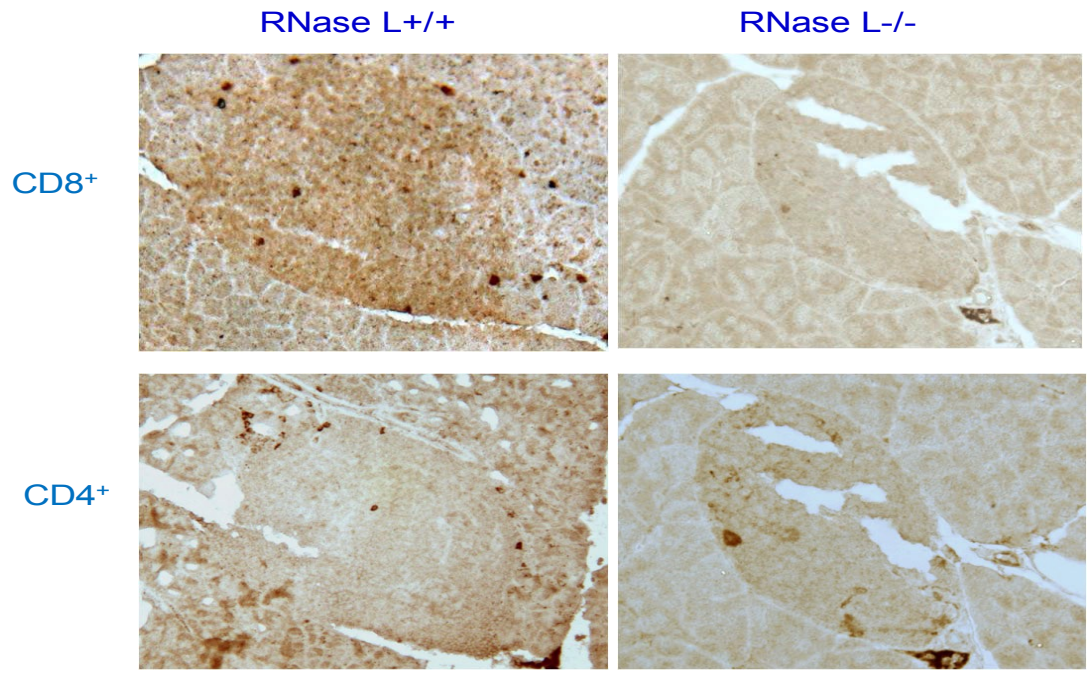

C.

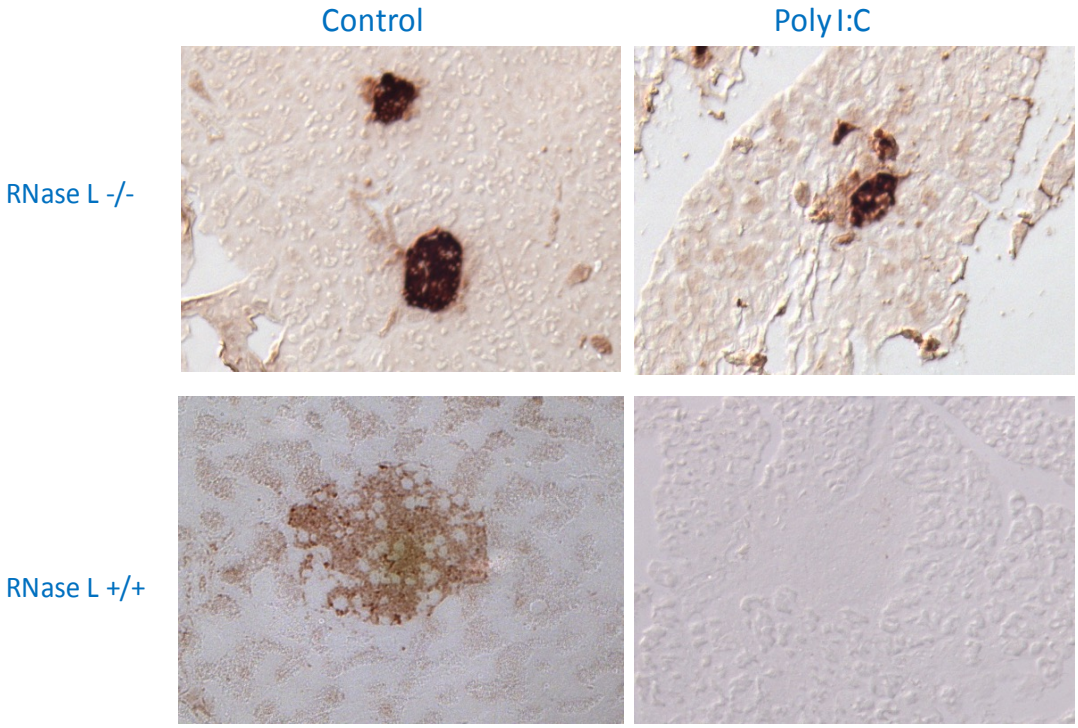

Figure 2-4. Infiltration of immune cells in the islets A. Hematoxlin and eosin stained pancreatic islets from B7.1-RL$^{+/+}$ and B7.1-RL$^{-/-}$ mice after treatment with or

without poly I:C. B. Immunohistological staining of $CD4^+$ and $CD8^+$ T cells in the islets from both types of mice after poly I:C treatment. C. Immunohistological staining of insulin in the islets from both types of mice before and after poly I:C treatment. Magnification x 40.

2.3.5 The expression of proinflammatory cytokines in the pancreatic tissues

In addition to IFN-α, several proinflammatory genes such as TNF-α, IL-1β and IFN-γ are believed to contribute to the development of type I diabetes [11, 12]. To determine if deficiency of RNase L results in any reduction of the expression of TNF-α, IL-1β, IL-6 and IFN-γ, RNase $L^{+/+}$ and $^{-/-}$ RIP-B7.1mice were treated with poly I:C at a concentration of 5 μg/g body weight every other days for a week and the level of these gene products in the pancreatic extracts was determined by ELISA. As shown in Figure 2-5, deficiency of RNase L reduced 37.5% and 48.5% of IFN-γ and TNF-α production respectively induced in the pancreas by poly I:C although the expression of IL-1β and IL-6 was found to be only slightly higher in the pancreas from RNase $L^{+/+}$ mice.

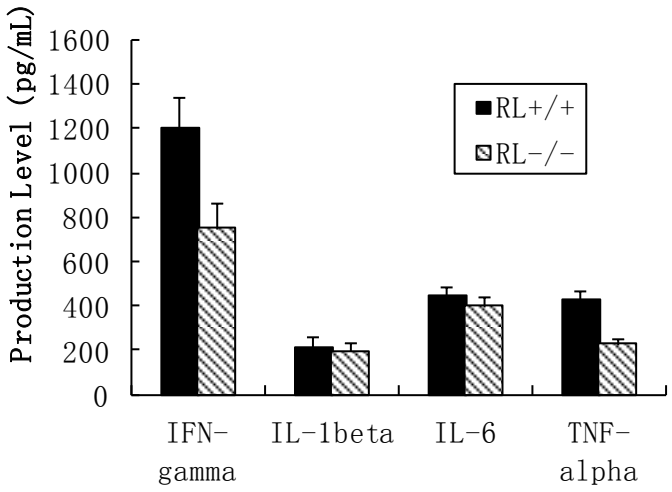

Figure 2-5. RNase L regulates the expression of proinflammatory genes RNase L deficient and wild type RIP-B7.1 mice were treated with poly I:C at a concentration of 5 μg/g body weight every other days for a week and the level of these factors in the pancreatic extracts was determined by ELISA using an ELISA kit for each of the analyzers. Experiments were performed two times in triplicates. Data are presented as mean ±SD.

2.4 Discussion and future studies

RNase L deficient mice RNase L null mice show enlarged thymus glands and increased T cell numbers at their early age, which likely results from reduced cell apoptosis, suggesting that RNase L may be involved in T cell development and functions. Indeed, skin allograft rejection is suppressed in mice lacking RNase L, implicating the involvement of RNase L in T cell immunity, particularly $CD4^+$ T-cell mediated immunity [28]. Alphavirus-based DNA vaccination against a non-mutated

tumor-associate self-antigen (tyrosinase-related protein-1, TRP-1) is severely impaired in RNase L null mice, indicating that RNase L plays an important role in host immune system against cancer [29]. Our study revealed that lymphocytes isolated from RNase L deficient mice displayed markedly attenuated cytotoxic activity (46% lower) against retinal endothelial cells (data not shown). B7-1 and B7-2 are homologous costimulatory ligands expressed on the surface of antigen presenting cells (APCs). Binding of these molecules to the T cell costimulatory receptors, CD28 and CTLA-4, is essential for the activation and regulation of T cell immunity [31]. Although expression of the B7.1 costimulator alone is not sufficient to induce diabetes in mice, β-cells expressing the molecule are more vulnerable to environmental harmful factors such as viral infection, resulting in destruction and leading to disease [32]. As a mimic of viral infection, poly I:C treatment alone can induce insulitis, but not diabetes in C57BL/6 mice. However, it can effectively induce diabetes in C57BL/6 mice expressing B7.1 on β-cells in the islets under a rat insulin promoter (RIP) [20]. In this study, we present evidence showing that RNase L deficient RIP-B7.1 mice display a significant delay of type I diabetes onset induced by poly I:C, suggesting that RNase L may be associated with the pathogenesis of this disease.

RNase L mediating IFN functions against viral infection and cell proliferation has been well established. A line of evidence has shown that IFN-α plays a vital role in

initiating autoimmune responses although the molecular mechanism is continuing to be a focus of investigation. Studies have revealed that type I diabetes onset in animal models induced by STZ and poly I:C is IFN-α dependent [19, 20]. In human, incidences in the development of type I diabetes have been widely documented during IFN-α therapy for viral infection such as hepatitis B and C viral infection [33, 34]. How IFN-α promoting the onset of type I diabetes remains to be further elucidated. RNase L is one of the key enzymes in the 2-5A system of IFN-α function. 2-5A activation of RNase L results in apoptosis in cells. It is believed that apoptosis is one of the key factors in triggering autoimmune responses in islets [35]. Thus, our results suggest that poly I:C treatment may induce an increase of IFN-α production in islets and subsequently activate the 2-5A system, leading to β-cell apoptosis, which further promotes the autoimmune responses, resulting in destruction of all β-cells and diabetes onset, and deficiency of RNase L in mice delays the onset of type I diabetes. Actually, this hypothesis is supported by a previous study which poly I:C induces cell apoptosis in pancreatic islets, resulting in release of islet autoantigens, triggering the autoimmune responses. In contrast, none of the bacterial products such as LPS and CpG are able to produce diabetes in these mice because they cannot induce islet cells to undergo overt apoptosis [36].

RNase L may directly be involved in the function of immune cells to impact the development of type I diabetes. Although T lymphocytes are primarily the effectors,

studies have indicated that B cells may play a vital role in the pathogenesis of autoimmune diseases. In NOD mice, the contribution of B cells was clearly demonstrated by the remarkable reduction in insulitis and diabetes incidence after B cell depletion using anti-IgM antibodies at birth or in NOD mice genetically deficient in B cells [37, 38]. By using the same animal model, studies have shown that B cells function as islet antigen–presenting cells for autoreactive T cells and produce antibodies which are directly pathogenic. In clinical trials, patients with type I diabetes treated with rituximab, a chimeric monoclonal antibody against the protein CD20 that is primarily found on the surface of B cells, displayed partially preserved β-cell function at one year post treatment as evidenced by decreasing C-peptide and less insulin requirements, suggesting an essential role of B cells in the development of this disease [39]. Interestingly, the population of $B220^+$/Ig D^+ double labeled B cells and $CD4^+$/$CD8^+$ double labeled T cells was 39% and 72% down after LPS treatment (Figure 2-4A) or 46% and 45% down after poly I:C treatment (Figure 2-4B) in the spleen of RNase L deficient mice, implicating that delayed onset of type I diabetes may be due to an attenuated immune responses as a result of that a harmful molecule such as LPS or poly I:C decreases the population of certain immune cells. The effect of RNase L on immunity is a focus of our investigation currently.

The production of proinflammatory genes in the islets plays a critical role in the pathogenesis of type I diabetes. It has been demonstrated that disruption of IFN-γ

function by using either IFN-γ specific Abs or soluble IFN-γ receptors (IFNγR) significantly reduces the incidence of spontaneous diabetes in NOD mice, implicating the importance of IFN-γ in the development of this disease [40, 41]. Complete protection from diabetes was observed when TNFR1, but not TNFR2 was knocked out in NOD mice although the direct effect of TNFR1 on β-cell death *in vivo* has not been defined clearly [42]. It has been reported that RNase L mediates the expression of certain genes through regulating RNA turnover [43, 44]. Our observation suggests that RNase L specifically regulating the expression of proinflammatory genes in the pancreas may contribute to type I diabetes onset induced by poly I:C. Thus, this study highlights the potential benefits of targeting RNase L in type I diabetes treatment.

2.5 References

[1] Choi, W. T., J An. Biology and clinical relevance of chemokines and chemokine receptors CXCR4 and CCR5 in human diseases. *Exp Biol Med.* 236(6):637-47, 2011.

[2] Asbun J, Villarreal FJ. The pathogenesis of myocardial fibrosis in the setting of diabetic cardiomyopathy, J Am Coll Cardiol. 47(4):693-700, 2006.

[3] Schnell O, The links between diabetes and cardiovascular disease, J Interv Cardiol.18:413-6. 2005.

[4] Russell TA, Diabetic nephropathy in patients with type 1 diabetes mellitus, Nephrol Nurs J. 33(1):15-28; quiz 29-30, 2006.

[5] Cara JF, Chaiken RL, Type 2 diabetes and the metabolic syndrome in children and adolescents, Curr Diab Rep. 6(3):241-50, 2006.

[6] www.cdc.gov/diabetes

[7] Zimmet P, Alberti KG and Shaw J, Global and societal implication of the diabetes epidemic, Nature, 414: 782-787, 2001.

[8] Mathis, et al., β-cell death during progress to diabetes, Nature, 414:792-797, 2001.

[9] Yoon JW and Jun HS, Cellular and molecular pathogenic mechanisms of insulin-dependent diabetes mellitus, Ann N Y Acad Sci. 928:200-11, 2001

[10] Mandrup-Poulsen T, Apoptotic signal transduction pathways in diabetes, Biochemical Pharmacology, 66:1433-1440, 2003.

[11] Anderson MS, Bluestone JA. The NOD mouse: a model of immune dysregulation. Annu Rev Immunol. 23:447-85, 2005.

[12] Solomon M, Sarvetnick N. The pathogenesis of diabetes in the NOD mouse. Adv Immunol. 84:239-64, 2004.

[13] Coppieters KT, Dotta F, Amirian N, Campbell PD, Kay TW, Atkinson MA, Roep BO, von Herrath MG. Demonstration of islet-autoreactive CD8 T cells in insulitic lesions from recent onset and long-term type 1 diabetes patients. J Exp Med. 209(1):51-60, 2012.

[14] Coppieters KT, von Herrath MG. Viruses and cytotoxic T lymphocytes in type 1 diabetes. Clin Rev Allergy Immunol. 41(2):169-78, 2011.

[15] Bergholdt R, et al., Type 1 database mellitus: an inflammatory disease of the islet, Adv Exp Med Biol. 552:129-53, 2004.

[16] Selmi C, Lleo A, Zuin M, Podda M, Rossaro L, Gershwin ME. Interferon alpha and its contribution to autoimmunity. Curr Opin Investig Drugs. 7(5):451-6, 2006.

[17] Chehadeh W, Weill J, Vantyghem MC, Alm G, Lefèbvre J, Wattré P, Hober D. Increased level of interferon-alpha in blood of patients with insulin-dependent diabetes mellitus: relationship with coxsackievirus B infection. J Infect Dis. 181(6):1929-39, 2000.

[18] Stewart TA, Hultgren B, Huang X, Pitts-Meek S, Hully J, MacLachlan NJ, Induction of type I diabetes by interferon-alpah in transgenic mice, Science, 260:1942-1946, 1993.

[19] Huang X, Hultgren B, Dybdal N, Stewart TA. Islet expression of interferon-alpha precedes diabetes in both the BB rat and streptozotocin-treated mice. Immunity. 1(6):469-78, 1994.

[20] Devendra D, Jasinski J, Melanitou E, Nakayama M, Li M, Hensley B, Paronen J, Moriyama H, Miao D, Eisenbarth GS, Liu E, Interferon-a as a mediator of polyinosinic:polycytidylic acid-induced type 1 diabetes, Diabetes, 54:2549-2556, 2005.

[21] Li Q, Xu B, Michie SA, Rubins KH, Schreriber RD, McDevitt HO. Interferon-alpha initiates type 1 diabetes in nonobese diabetic mice. Proc Natl Acad Sci U S A. 105(34):12439-44, 2008.

[22] Zhou A, Hassel BA, Silverman RH, Expression cloning of 2-5A-dependent RNAase: a uniquely regulated mediator of interferon action, Cell, 72(5):753-765, 1993.

[23] Silverman RH, 2-5A dependent Rnase L: A regulated endoribonuclease in the IFN system, D'alessio G, Riordan JF (eds) "Ribonucleases:structure and function", New York: Academic Press, Inc. pp 517-547, 1996.

[24] Zhou A, Paranjape JM, et al. Impact of RNase L overexpression on viral and cellular growth and death. JICR, 18(11): 953-61, 1998.

[25] Hassel BA, Zhou A, Sotomayor C, Maran A, Silverman RH, A dominant negative mutant of 2-5A-dependent RNase suppresses antiproliferative and antiviral effects of IFN. EMBO J 12: 8, 3297-304, 1993.

[26] Zhou A, Paranjape J, Brown TL, Nie H, Naik S, Dong B, Chang A, Trapp B, Fairchild R, Colmenares C, Silverman RH, IFN action and apoptosis are defective in mice devoid of 2',5'-oligoadenylate-dependent RNase L., EMBO J 16(21): 6355-6363, 1997.

[27] Bonnevie-Nielsen V, Martensen PM, Justesen J, Kyvik KO, Kristensen B, Levin K, Beck-Nielsen H, Worsaa A, Dyrberg T, The antiviral

2’,5’-oligoadenylate synthetase is persistently activated in type 1 diabetes, Clinical Immunology, 96:11-18, 2000.

[28] Silverman RH, Zhou A, Auerbach MB, Kish D, Gorbachev A and Fairchild RL , Skin Allograft Rejection is Suppressed in Mice Lacking the Antiviral Enzyme, 2',5'-Oligoadenylate Dependent RNase L, Viral Immunology, 15:77-83, 2002.

[29] Leitner WW, Hwang LN, DeVeer ML, Zhou A, Silverman RH, Williams BRG, Dubensky TW, Ying H and Nicholas P. Restifo, Alphavirus-based DNA vaccine breaks immunological tolerance by activating innate antiviral pathways” Nature Medicine, 9:33-39, 2003.

[30] Nolan-Sorden NL, Lesiak K, Bayard B, Torrence PF, Silverman RH, Photochemical crosslinking in oligonucleotide-protein complexes between a bromine-substituted 2-5A analog and 2-5A-dependent RNase by ultraviolet lamp or laser, Anal Biochem 184(2): 298-304, 1990.

[31] Greenwald RJ, Freeman GJ, Sharpe AH. The B7 family revisited. Annu Rev Immunol. 23:515-48, 2005.

[32] Wong S, Guerder S, Visintin I, Reich EP, Swenson KE, Flavell RA, Janeway CA Jr. Expression of the co-stimulator molecule B7-1 in pancreatic beta-cells accelerates diabetes in the NOD mouse. Diabetes. 44(3):326-9, 1995.

[33] Kose S, Gozaydin A, Akkoclu G, Ece G. Chronic hepatitis B with type I diabetes mellitus and autoimmune thyroiditis development during interferon alpha therapy. J Infect Dev Ctries. 6(4):364-8, 2012.

[34] di Cesare E, Previti M, Russo F, Brancatelli S, Ingemi MC, Scoglio R, Mazzù N, Cucinotta D, Raimondo G. Interferon-alpha therapy may induce insulin autoantibody development in patients with chronic viral hepatitis. Dig Dis Sci. 41(8):1672-7, 1996.

[35] Kawazoe T, Araki M, Lin Y, Ogawa M, Okamoto T, Yamamura T, Wakakura M, Murata M. New-onset type 1 diabetes mellitus and anti-aquaporin-4 antibody positive optic neuritis associated with type 1 interferon therapy for chronic hepatitis C. Intern Med. 51(18):2625-9, 2012.

[36] Maniati E, Potter P, Rogers NJ, Morley BJ. Control of apoptosis in autoimmunity. J Pathol. 214(2):190-8, 2008.

[37] Marino E, Silveira PA, Stolp J, Grey ST. B cell-directed therapies in type 1 diabetes. Trends Immunol, 32:287–294, 2011.

[38] Silveira PA, Grey ST. B cells in the spotlight: innocent bystanders or major players in the pathogenesis of type 1 diabetes. Trends Endocrinol Metab 17:128–135, 2006.

[39] Pescovitz MD, Greenbaum CJ, Krause-Steinrauf H, Becker DJ, Gitelman SE, Goland R, Gottlieb PA, Marks JB, McGee PF,Moran AM, Raskin P, Rodriguez H, SchatzDA, Wherrett D, Wilson DM, Lachin JM, Skyler JS. Rituximab,

B-lymphocyte depletion, and preservation of beta-cell function. N Engl J Med 361:2143–2152, 2009.

[40] Campbell IL, Kay TW, Oxbrow L, Harrison LC. Essential role for interferon-gamma and interleukin-6 in autoimmune insulin-dependent diabetes in NOD/Wehi mice. J Clin Invest. 87(2):739-42, 1991.

[41] Nicoletti F, Zaccone P, Di Marco R, Di Mauro M, Magro G, Grasso S, Mughini L, Meroni P, Garotta G.The effects of a nonimmunogenic form of murine soluble interferon-gamma receptor on the development of autoimmune diabetes in the NOD mouse. Endocrinology. 137(12):5567-75, 1996.

[42] Kägi D, Ho A, Odermatt B, Zakarian A, Ohashi PS, Mak TW. TNF receptor 1-dependent beta cell toxicity as an effector pathway in autoimmune diabetes. J Immunol. 162(8):4598-605, 1999.

[43] Bisbal C, Silhol M, Laubenthal H, Kaluza T, Carnac G, Milligan L, Le Roy F, Salehzada T, The 2'-5' oligoadenylate/RNase L/RNase L inhibitor pathway regulates both MyoD mRNA stability and muscle cell differentiation, Mol Cell Biol, 20(14): 4959-4969,2000.

[44] Chandrasekaran K, Mehrabian Z, Li XL, Hassel B, RNase L regulates the stability of mitochondrial DNA-encoded mRNAs in mouse embryo fibroblasts, Biochem Biophy Res Comm, 325:18-23, 2004.

CHAPTER III

QUANTITATIVE DETERMINATION OF HYM3 WITH LC-MS/MS

3.1 Introduction

Various steroidal derivatives have an anticancer effect. 6-Hydroximino-4-aza-A-homo-cholest-3-one was found to be an effective drug candidate. In this study, an analytical method has been developed to study the pharmacokinetics and pharmacodynamic aspects of the drug candidate, and its metabolism characteristics in mice. This project involved development and validation of a rapid and sensitive LC-MS/MS method for determination of the compound in mouse plasma. Method validation was fully performed according to the FDA guidelines.

3.1.1 Method Summary

Sample preparation was realized by a protein precipitation procedure, and LC was performed by using a Phenomenex-Kinetex-C8 column with a gradient mobile phase of 0.2% formic acid in water and 0.2% formic acid in acetonitrile at a rate of 0.2 ml/min. For measurement, 10 μL of the supernatant was injected onto LC/MS system consisting of a Shimadzu Prominence HPLC and an AB Sciex QTrap 5500 mass spectrometer with positive electrospray ionization. A MRM mode was chosen for sensitive and specific detection of the analyte and internal standard. The method developed has been validated in mouse plasma according to the FDA guidance. The quantitative assessment of Hym3 fills the gap of lacking analytical method for the pharmacokinetic studies.

3.2 Material and methods

3.2.1 Chemicals and solutions

Hym3 and (3E)-hydroximinocholest-6-one, an internal standard (IS), were kindly provided by the College of Chemistry and Life Science, Guangxi Teachers Education University (Nanning, China). Deionized water was collected from the Barnstead NANOpure® water purification system (Thermo Scientific, Waltham, MA, USA). Formic acid was purchased from Acros (Morris Plains, NJ, USA). Dimethylsulfoxide (DMSO), HPLC-grade acetonitrile and ethyl acetate were obtained from Sigma–

Aldrich (St. Louis, MO, USA). Pooled blank mouse plasma was from Equitech-Bio (Kerrville, TX, USA).

Hym3 and IS stock solutions were prepared according to the following procedure: first, the compounds were weighted out by an analytical balance and dissolved separately into acetonitrile to a concentration of 1.00 mg/mL. For Hym3, the stock solution was transferred into 1.5-mL microcentrifuge tubes as per aliquot of 100 μL. For the IS, the stock solution was divided evenly into 25 μL per tube. Afterward, the solution in the microcentrifuge tubes was dried in a DNA120 SpeedVac® (ThermoSavant, Hollbrook, NY, USA) vacuum evaporator at 25℃ and the dried stocks were kept at −20℃ until use. Before use, 1.00 mL of deionized water was added into the microcentrifuge tube to make the working solution of Hym3 and IS at 100 and 25.0 μg/mL, respectively. The Hym3 and the IS working solutions were freshly prepared before analysis. The mobile phase of LC was prepared by a gradient mobile phase of 0.2% formic acid in water and 0.2% formic acid in acetonitrile at a rate of 0.2 ml/min.

3.2.2 LC-MS/MS instrumentation

The LC–MS/MS system was composed by a Shimadzu Prominence HPLC and an AB Sciex QTrap 5500 mass spectrometer (AB Sciex, Toronto, Canada) with positive

electrospray ionization. The HPLC unit included two binary pumps, a degasser, an autosampler, an inline Phenomenex filter (0.5 μm pore) a Phenomenex Kinetex C8 column (50x2.1 mm, 2.6μ) (Torrance, CA, USA) and Analyst software version 1.4.2 was utilized for the LC–MS/MS system operation, data acquisition and processing. For each LC-MS/MS analysis, the injection volume of the sample onto the column was 10 μL. Isocratic elution was utilized in the chromatographic separation. The flow rate was set as 200 μL/min. The post-column switching valve was programmed so that only the column eluate after 5.0 min was diverted to the mass spectrometer for analysis. The positive electrospray- ionization (ESI+) mode was adopted when operating the mass spectrometer. The mass spectrometer was tuned by direct infusion of a solution containing 10.0 μg/mL of Hym3 and 10.0 μg/mL of IS dissolved in the mobile phase. The flow rate of infusion was set as 3 μL/min with a syringe pump (Harvard Apparatus, South Natick, MA, USA). Full mass spectrometric scans of HyM3 and IS showed protonated molecular ions of 431 and 416 m/z, and fragmentation of these two precursor ions revealed predominant product ions of 370 and 344 m/z respectively. MRM channels were set at m/z 431→370 for HyM3 and 416→344 for IS. The optimized parameters for detecting Hym3 and IS were set as following: the ion spay voltage (IS) was 5500 eV; the temperature was at 300℃; the heating gas (GS1), nebulization gas (GS2), and Curtain gas (CUR) were 45, 45, and 20 psi, respectively. Compound parameters, including declustering potentials (DP), entrance potential (EP), collision energy (CE), and collision exit potential (CXP) for both Hym3 and IS were set at 90, 7.0, 15.0, and 20V, respectively.

3.2.3 Preparation of standard solutions and plasma controls

Hym3 standard solutions at the concentration of 10.0, 20.0, 40.0, 100.00, 200.0, 400.0, 1000.0, 2000, and 4000 ng/mL were prepared by a serial dilution of 100 μg/mL Hym3 working solution. The IS was diluted from the 100 μg/mL working solution to 400.0 ng/mL.

The calibrators (0.500, 1.00, 2.00, 5.00, 10.0, 20.0, 50.0, 100, and 200 ng/mL) of Hym3 in mouse plasma were obtained individually by mixing 200 μL of pooled blank plasma, together with 5.0 μL of Hym3 standard solution (at twenty times of the concentration of the related calibrator) and 10.0 μL of IS standard solution at 400 ng/mL.

3.2.4 Protein precipitation of Hym3

Plasma calibrators, controls and animal samples were extracted by using a protein precipitation protocol: 800 of ACN were mixed with the plasma sample in a 1.5mL microcentrifuge tube. Then, the sample was subjected to a short vortex for 1 min, followed by a centrifugation at 13000×g for 10 min. Next, 85% of the organic (upper) layer (ca. 850 μL) was transferred into a clean 1.5-mL microcentrifuge tube and dried

by vacuum evaporation on the DNA 120 SpeedVac® at 25 ℃. The sample residue was finally reconstituted with 850 μL of deionized water.

3.2.5 Matrix effect and recovery studies

To study the matrix effect, 200 μL pooled blank plasma mixed with 10 μL of water was extracted with the protocol described in Section 3.2.4. Afterward, a mixture of Hym3 and the IS standard solutions were spiked into the post-extract matrix. The prepared samples possessed Hym3 of 1.25, 15.0 and 180 ng/mL, and the IS of 20.0 ng/mL. The peak area ratios of Hym3 to IS in the spike-after-extraction (SAE) standards were compared with those of the corresponding authentic pure standards.

To obtain the recovery data, Hym3 plasma calibrators (1.25, 15.0 and 180 ng/mL, with the IS at 20.0 ng/mL) were analyzed. IS normalized recovery of Hym3 was calculated by comparing the peak area ratios of Hym3 to IS in the plasma calibrators with those of the corresponding SAE standards. The absolute recovery of the IS was obtained by comparing the peak areas of the IS in the plasma calibrators with those of the corresponding SAE standards.

3.2.6 Stability studies

Mouse plasma test controls (1.25 and 180 ng/mL) were prepared as described in Section 3.2.3 except the IS standard was added prior to the LLE. All experiments were run in triplicate and the results were compared with freshly prepared plasma controls. For the freeze and thaw stability study, the test controls were undergone three freeze and thaw cycles. In each cycle, the test controls were frozen at −20℃for at least 24 h and thawed at room temperature without help. The short-term temperature stability study was carried out by leaving the test controls at the room temperature (25℃) for 4–24 h. For the long-term stability, the test controls were stored at −20℃ for 90 days prior to analysis.

3.3 Results and discussions

3.3.1 Method development

Mass spectrometric detection of Hym3 and the IS

In this study, “auto-tune” function of the analyst software was utilized for the instrument response optimization. Due to their chemical properties, Hym3 and the IS can form protonated species more easily than the deprotonated species through electrospray ionization. Thus, the positive electrospray ionization mode was utilized for the identification and quantification of Hym3 and the IS. Figure 3.1 A and B

demonstrates the predominant molecular ions of Hym3 and the IS at m/z 431 for $[Hym3+H]^+$ and m/z 416 $[IS+H]^+$, respectively. With collision-induced-dissociation (CID) introduced by argon gas in the second quadrupole, these two molecular ions were further dissociated into product ions illustrated in Figure 3.1 C and D, respectively. The major product ion of the protonated Hym3 and the IS were shown at m/z 370 and m/z 344, respectively. As a result, MRM channels were set at m/z 431→370m/z for HyM3 and 416→344 m/z for the internal standard. To understand the fragmentation mechanisms in CID, the m/z difference of the compound before and after CID were compared. Summarized with the structural information of the compounds, the proposed fragmentation mechanism is shown in Figure 3-2.

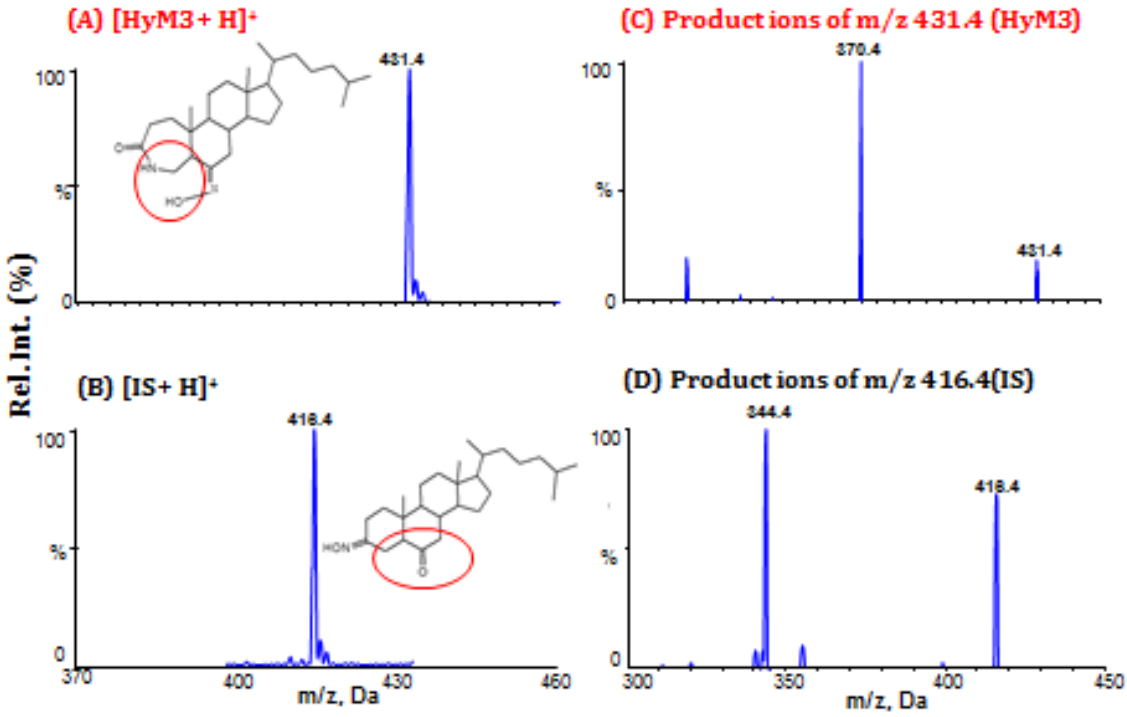

Figure 3-1. The mass spectra of Hym3 and the internal standard

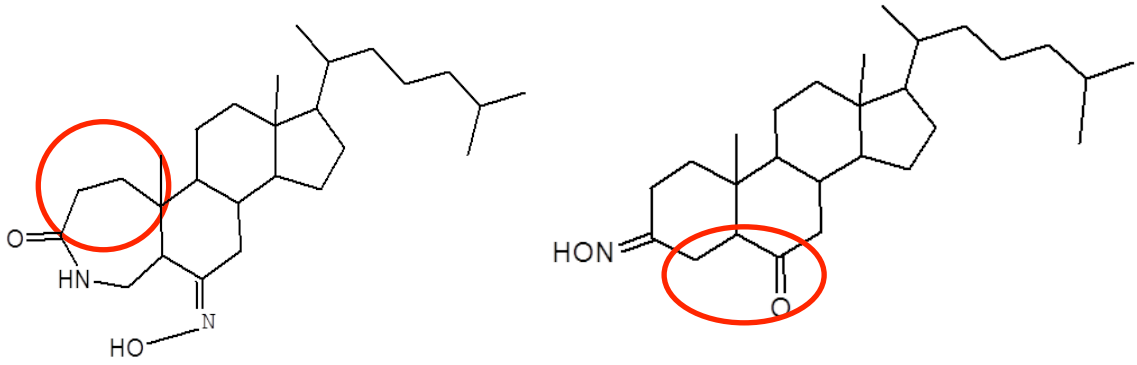

Figure 3-2. The proposed fragmentation bonds of Hym3 and the IS.

LC separation of Hym3

Both compounds can be considered as more hydrophobic than hydrophilic. Based on this information, three C-18 reverse phase columns, a Phenomenex Gemini® columns (2.0mm×50mm, 5 µm particle size with 110Å pore size) and a YMC ODS-AQ® column (2.0mm×50mm, 5 µm particle size with 120Å pore size) and a C8 a Phenomenex Kinetex C8 column (50x2.1 mm, 2.6µ) have been tried for optimized LC separation. Both columns successfully retained Hym3 and the IS on the column for over 3 column volumes and were able to provide base line separation between Hym3 and the IS. However, the Phenomenex Kinetex C8 column was able to provide better peak shape compared to the other columns. Meanwhile, since Hym3 and the IS are basic compounds, 0.2% of formic acid was added into the mobile phase in order to facilitate the protonation of the analytes, which enhanced the sensitivity of MS detection.

The increased hydrophilicity of the analyte after the addition of the formic acid also reduced the retention times of the analyte and the IS, leading to shorter retention time and faster LC analysis.

To optimize the separation efficiency, the percentage of acetonitrile in the mobile phase was adjusted. Although a complete baseline resolution between Hym3 and the IS could be achieved with a mobile phase consisted of 35.0% acetonitrile, 0.2% formic acid and 65% deionized water (v/v/v), the total LC time was as long as 5 min, but the Matrix effect was too big to use the isocratic elution. To eliminate the interferences between the two compounds, a gradient mobile phase of 0.2% formic acid in water and 0.2% formic acid in acetonitrile at a rate of 0.2 ml/min was applied (Figure 3-3).

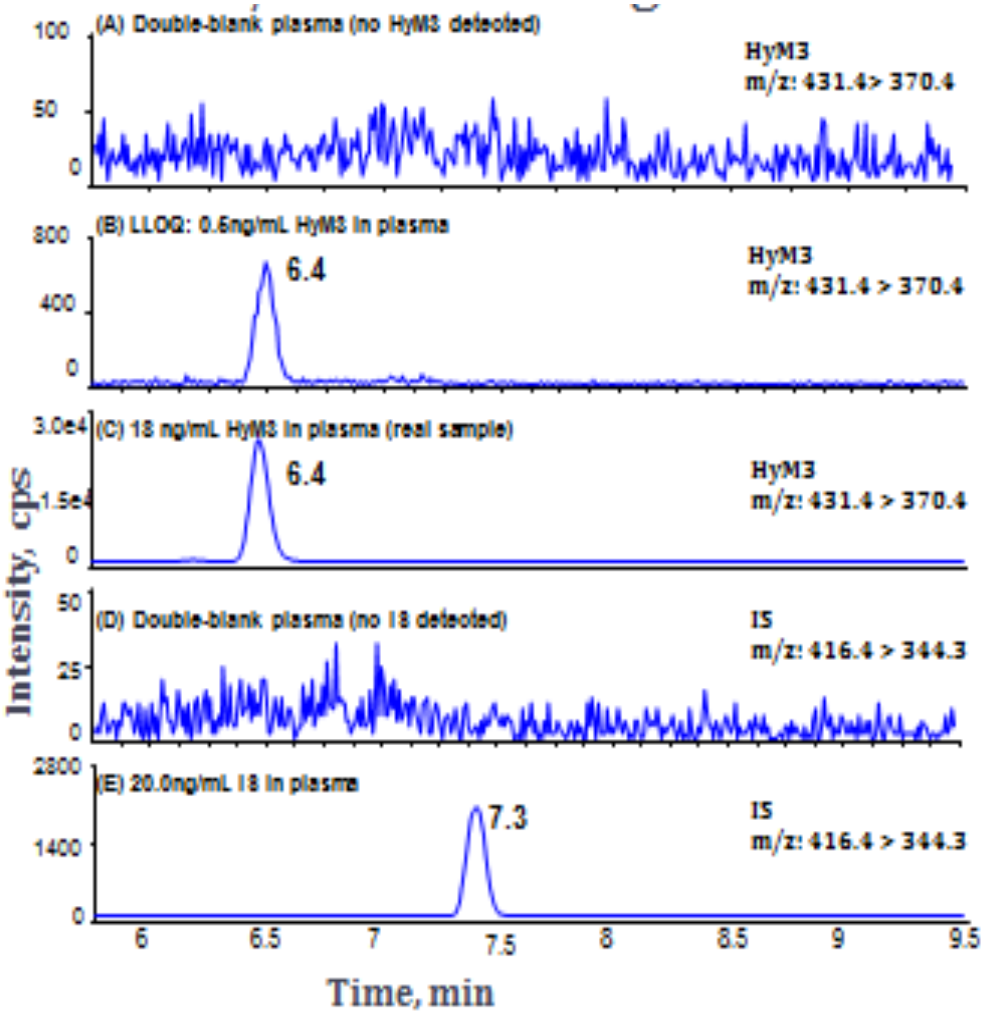

Figure 3-3. Representative MRM chromatograms of analytes in mouse plasma.

Fig.3-3 Representative MRM chromatograms of analytes in mouse plasma (A) double-blank plasma (no Hym3 detected); (B) 0.50 ng/mL Hym3 in plasma (at LLOQ with a S/N of 17.2); (C) 18.0 ng/mL Hym3 in plasma; (D) double-blank plasma (no IS detected); and (E) 20 ng/mL IS in plasma.

3.3.2 Method validation

The performance of the method developed was validated according to the FDA guidance for industry bioanalytical method validation [1].

Matrix effect and recovery studies

In the studies of matrix effect and recovery, triplicate measurements were performed for each of three different concentration levels (i.e., low, medium, and high). The matrix effect was normalized by the signal of the Matrix Factor of IS (MF_{IS}), and thus was calculated with the equation as following:

$$MF_{IS} = \frac{(A/A')_{matrix}}{(A/A')_{solvent}}$$

A represents the peak area of the analyte; while A' indicates the peak area of the IS. (A/A') indicates the peak area ratio of the analyte to the IS. Thus, $(A/A')_{matrix}$ indicates the peak area ration in the post-extraction matrix and $(A/A')_{solvent}$ indicates that in pure solvent.

As Table 3-1 illustrated, the MF_{IS} in mouse plasma matrices varied between 1.03-1.10. Meanwhile, the values of MF_{IS} were quite consistent over the concentration range reproducible with standard deviation (SD) $\leqslant$0.02.

To reduce the variation caused by instrument, the recovery was also studies as the IS normalized form (R_{IS}). It was calculated with the equation below:

$$RC_{IS} = \frac{(A/A')_{extraction}}{(A/A')_{matrix}} \times 100\%$$

$(A/A')_{extraction}$ represents the peak area ratio in extracted plasma samples.

The summarized recovery data can be viewed in Table 3-1. The values ranged from 97 to 98%. The absolute recoveries (RC') of the IS from both plasma samples were also calculated by using the equation below:

$$RC' = \frac{A'_{extraction}}{A'_{matrix}} \times 100\%$$

Here $A'_{extraction}$ stands for the peak area of the IS in the extracted plasma sample; while A'_{matrix} represents the peak area of the IS in the post-extraction matrix. The values of RC' ranged from 96 to 99% in mouse plasma and the results were reproducible and consistent within the calibration range.

Table 3-1. Matrix effect and recovery

[Hym3] (ng/mL)	Recovery± SD （%）	MF_{IS} ± SD
Low QC	97±1	1.10 ± 0.02
Mid QC	98±2	1.03 ± 0.02
High QC	97±2	1.04 ± 0.02

Calibration of curve, accuracy, and precision

The calibration curve of Hym3 in mouse plasma was established with nine non-zero plasma calibrators. For each set of calibrator, one double-blank (with neither Hym3 nor IS) plasma sample and one zero (with IS only) plasma sample were also included. The concentrations of Hym3 for the non-zero calibrators were 0.50, 1.00, 2.00, 5.00, 10.0, 20.0, 50.0, 100 and 200 ng/mL. The linear calibration curves ranged from 0.50 to 200 ng/mL were established by plotting A/A' in mouse plasma versus the concentrations of Hym3. The weighting factor for both calibration curves were utilized as 1/x (the reciprocal of Hym3 concentration). Both calibration data were given in Table 3-2. In the determination of the lower limits of quantification (LLOQ), the plasma calibrator with the lowest concentration, yet still fit in the calibration curve with acceptable accuracy and precision. The concentrations of the calibrators were back-calculated according to the calibration equation with the information of the A/A'. The accuracy and precision were calculated as they have been described in the previous chapter. The accuracy and precision for the mouse plasma ranged from 1 to 3% and from 3 to 5%, respectively. All values fell within the acceptable criteria (i.e., $\leqslant \pm 15\%$ at all concentrations except at LLOQ where $\leqslant \pm 20\%$) suggested by the FDA guidance.

The precision of the method was evaluated in two aspects: the intra-and inter assay precisions. To determine the precisions, five replicates of plasma control samples at

low-, mid- and high-concentration levels (LQC, MQC and HQC) were prepared and analyzed. The accuracies of the above studies were between 1 to 4% (Table 3-3). As expected, they fell well within the acceptable criteria suggested by the FDA guidance.

Table 3-2. Data for calibration equations of Hym3 in mouse plasma

Sample Matrix	Nominal [Hym3] (ng/mL)	Measured [Hym3] (ng/mL)	SD (ng/mL)	Precision (%CV)[a]	Accuracy (%RE)[b]
Plasma	0.50	0.50	0.01	4	1
	1.00	0.98	0.03	3	-2
	2.00	2.02	0.08	4	1
	5.00	5.04	0.13	5	1
	10.0	9.90	0.39	4	-1
	20.0	19.5	0.5	3	-2
	50.0	48.9	1.9	4	-3
	100	103	4	3	3
	200	202	2.5	5	1

Calibration Equations: Mouse plasma: $Y = 0.0385 (\pm 0.012)\ x - 0.00107 (\pm 0.00304)$ ($r^2 = 0.999 \pm 0.000$)

Each measured concentration was based on three measurements carried out on three different days and the S.D. values showed in the table indicated the standard deviation of each triplicate measurement. The calibration equations were based on three separate measurements carried out on three different days.

Table 3-3. Accuracy, intra- and inter-assay precisions of Hym3 in mouse plasma.

Plasma	LQC	MQC	HQC
Accuracy(%)	3	1	2
Intra-assay Precision(%),n=5	4	2	1
Inter-assay precision(%),n=5	2	1	2

The concentration of LQC, MQC and HQC of Hym3 were 1.25, 15 and 180 ng/mL, respectively. The concentration of IS was 20.0ng/mL.

Stability studies

Two concentration levels, 1.25 and 180 ng/mL, were utilized in the stability test. Triplicate measurements were performed at each concentration level. The stability results were summarized in Table 3-4. As shown in the table, no significant loss of Hym3 was observed in mouse plasma under the storage conditions and its recovery ranged between 96 and 98% after stored at room temperature for 24 h and three freeze-and-thaw cycles. In addition, a long-term storage of HYM3 in mouse plasma at -20 ℃ also showed adequate recoveries. Based on these experimental facts, we conclude that Hym3 is pretty stable in either its stock solution or the spiked mouse plasma, which is important for deciding the operative time in pharmacokinetic study of the drug candidate in the future.

Table 3-4. Stability data of Hym3 under different test conditions

Test conditions	Temperature (° C)	Nominal [analyte] (ng/mL)	Recovery ± SD (%) (n = 3)
Stock solution (30 days)	23	1.00 X 10^6	99 ± 1
Bench-top 24hrs	23	Low QC	92 ± 1
		High QC	94 ± 2
Post-extraction bench-top 12hrs	23	Low QC	98 ± 2
		High QC	96 ± 1
3 Freeze-thaw cycles	-20 - 23	Low QC	101 ± 2
		High QC	97 ± 3

3.3 Conclusions and future studies

Based on all the experimental data as described above, a quantitative LC–MS/MS method for the assessment of Hym3 in mouse plasma has been developed. In brief, the analytes in mouse plasma were extracted by ethyl acetate, separated by Phenomenex Kinetex C8 column (50x2.1 mm, 2.6μ), and then analyzed through the tandem mass spectrometry. Method validation has been performed in mouse plasma according to the FDA guidance. The linear range of the method was from 0.50 to 200ng/mL in mouse plasma. Due to its high accuracy, precision, and sensitivity, the method will be useful for studying pharmacokinetics and pharmacodynamics of Hym3 in its preclinical and clinical trials as a potent drug candidate for cancer treatment in the future.

3.4 References

[1] U.S. Food and Drug Administration (FDA) & Center for Drug Evaluation and Research (CDER), Guidance for Industry: Bioanalytical Method Validation, available at http://www.fda.gov/cder/guidance/4252fnl.htm, 2001.

[2] B.M. Chassy, R.J. Suhadolnik, J Biol Chem. 242 (1967) 3655.

[3] M.H. Iltzsch, S.S. Uber, K.O. Tankersley, M.H. el Kouni, Biochem. Pharmacol. 49 (1995) 1501.

[4] M.H. el Kouni, V. Guarcello, O.N. Al Safarjalani, F.N. Naguib, Antimicrob. Agents. Chemother. 43 (1999) 2437.

[5] J.P. Dubey, C.P. Beattie. Toxoplasmosis of animals and man, CRC Press, Boca Raton, FL, 1988, p. 1.

[6] P.D. Walzer, R.M. Genta (Eds.), Parasitic infections in the compromised host, Marcel Dekker, New York, NY, 1989, p. 179.

[7] D.N. Wald, H.M. Vermaat, S. Zang, A. Lavik, Z. Kang, G. Peleg, S.L. Gerson, K.D. Bunting, M.L. Agarwal, B.L. Roth, W. Tse, Cancer Res. 68 (2008) 4369.

[8] American Society of Clinical Oncology, Leukemia - Acute Myeloid: overview, available at: http://www.cancer.net/patient/Cancer+Types/Leukemia+-+Acute+Myeloid+-+AML.

[9] E. Estey, H. Döhner, Lancet. 368 (2006) 1894.

[10] B. Steffen, C. Müller-Tidow, J. Schwäble, W.E. Berdel, H. Serve, Crit Rev Oncol. Hematol. 56 (2005) 195.

[11] Z.Y. Wang, Z. Chen, Blood. 111(2008):2505.

[12] M.S. Tallmann, Ann Hematol. 83 (2004) S81.

[13] R.H. Rais, O.N. Al Safarjalani, V. Yadav, V. Guarcello, M. Kirk, C.K. Chu, F.N. Naguib, M.H. el Kouni, Biochem. Pharmacol. 69(2005) 1409.